Tectonic development of the Samail ophiolite: High-precision U-Pb zircon geochronology and Sm-Nd isotopic constraints on crustal growth and emplacement

Matthew Rioux,[1,2] Samuel Bowring,[1] Peter Kelemen,[3] Stacia Gordon,[4] Robert Miller,[5] and Frank Dudás[1]

Received 11 July 2012; revised 13 December 2012; accepted 18 February 2013; published 29 May 2013.

[1] New high-precision single grain U-Pb zircon geochronology and whole rock Nd isotopic data provide insight into the magmatic and tectonic development of the Samail ophiolite. The analyzed rocks can be broadly divided into two groups based on their structural position, dates, and isotopic composition: an older group related to on-axis magmatism and a younger group of post-ridge dikes, sills, and stocks. On-axis gabbros, tonalites and trondhjemites yielded Th-corrected $^{206}Pb/^{238}U$ dates from 96.441 ± 0.062 to 95.478 ± 0.056 Ma. These dates, combined with dates from *Rioux et al.* (2012), suggest that most of the ophiolite crust formed at an oceanic spreading center in <1 Ma. The post-ridge intrusions come from all depths in the crust, the upper mantle, and the metamorphic sole. Post-ridge gabbros, tonalites, and trondhjemites from the crust and mantle yielded Th-corrected $^{206}Pb/^{238}U$ dates of 95.405 ± 0.062 to 95.077 ± 0.062 Ma. A small trondhjemitic pod from the metamorphic sole yielded younger Th-corrected $^{206}Pb/^{238}U$ dates of 94.90 ± 0.38 to 94.69 ± 0.12 Ma. Isotopic data suggest two distinct sources for the post-ridge magmas: five of the gabbros and tonalites from the crust have ε_{Nd}(96 Ma) = 6.90 ± 0.12 to 7.88 ± 0.16, and two trondhjemites from the upper mantle and metamorphic sole have ε_{Nd}(96 Ma) = −7.77 ± 0.08 and −7.01 ± 0.16. The negative ε_{Nd}(t) and U-Pb dates from the mantle dike require that subduction or thrusting was established below the ophiolite ≤0.25–0.5 Ma after formation of the crust. The bimodal isotopic composition of post-ridge magmas may reflect coeval decompression and/or fluid fluxed melting of the mantle and melting, dehydration, or assimilation of sediment in the down going plate at this time. The new data place temporal constraints on mid-ocean ridge and supra-subduction zone models for ophiolite formation.

Citation: Rioux, M., S. Bowring, P. Kelemen, S. Gordon, R. Miller, and F. Dudás (2013), Tectonic development of the Samail ophiolite: High-precision U-Pb zircon geochronology and Sm-Nd isotopic constraints on crustal growth and emplacement, *J. Geophys. Res. Solid Earth*, *118*, 2085–2101, doi:10.1002/jgrb.50139.

1. Introduction

[2] The Samail ophiolite in Oman and the United Arab Emirates (UAE) is one of the largest, best exposed, and best studied ophiolites on Earth. The structure of the ophiolite makes it clear that the crust formed in an extensional environment similar to modern fast-spreading mid-ocean ridges (MOR), making it an invaluable resource for studying MOR processes. However, many researchers have highlighted evidence for a complex tectonic environment during formation of the crust [*Boudier et al.*, 1997; *MacLeod and Rothery*, 1992; *Nicolas and Boudier*, 1995; *Nicolas et al.*, 2000; *Reuber et al.*, 1991] and demonstrated important differences between the Samail ophiolite and modern ridges, including geochemical differences between MOR basalts and lavas in the ophiolite [*Alabaster et al.*, 1982; *Ernewein et al.*, 1988; *Godard et al.*, 2003; *MacLeod et al.*, 2013; *Pearce et al.*, 1981] and the presence of multiple generations of plutonism and volcanism within the mantle and crust [*Adachi and Miyashita*, 2003; *Alabaster et al.*, 1982; *Ernewein et al.*, 1988; *Godard et al.*, 2003; *Godard et al.*, 2006; *Goodenough et al.*, 2010; *Juteau et al.*, 1988b; *Pearce et al.*, 1981; *Tamura and Arai*, 2006]. To determine how observations from the ophiolite can be applied to modern spreading

Additional supporting information may be found in the online version of this article.

[1]Department of Earth, Atmospheric, and Planetary Sciences, Massachusetts Institute of Technology, Cambridge, Massachusetts, USA.
[2]Now at Earth Research Institute, University of California Santa Barbara, Santa Barbara, California, USA.
[3]Department of Earth and Environmental Studies, Columbia University, Lamont Doherty Earth Observatory, Palisades, New York, USA.
[4]Department of Geological Sciences and Engineering, University of Nevada, Reno, Nevada, USA.
[5]Geology Department, San Jose State University, San Jose, California, USA.

Corresponding author: M. Rioux, Earth Research Institute, University of California, Santa Barbara, CA 93106, USA. (rioux@eri.ucsb.edu)

2169-9313/13/10.1002/jgrb.50139

centers and to understand the origin of ophiolites, it is necessary to reconstruct the tectonic and magmatic history during formation and emplacement of the ophiolite.

[3] We have used high-precision single grain U-Pb zircon geochronology and whole rock Sm-Nd isotopic data from gabbros, tonalites, and trondhjemites to study these processes. In *Rioux et al*. [2012a], we reported dates from 12 mostly gabbroic rocks from a well-exposed crustal section at the center of the Wadi Tayin massif. Here we present new dates from seventeen gabbros, tonalites, trondhjemites, and a granite from five massifs along two thirds of the length of the ophiolite. In addition, we report whole rock Sm-Nd isotopic data from eight of the sample locations. The new data suggest that crustal growth by ridge magmatism in the ophiolite occurred between 96.441 ± 0.062 to 95.478 ± 0.056 Ma. The ophiolite mantle and crust were subsequently intruded by a secondary magmatic series related to subduction or thrusting below the ophiolite between 95.405 ± 0.062 and 95.077 ± 0.062 Ma, and small volume melting of the preserved metamorphic sole persisted until at least 94.90 ± 0.38 to 94.69 ± 0.12 Ma.

2. Geology of the Samail Ophiolite

[4] The Samail ophiolite preserves oceanic lithosphere formed at a Cretaceous fast-spreading ridge [*MacLeod and Rothery*, 1992; *Nicolas*, 1989; *Nicolas et al*., 1996; *Rioux et al*., 2012a; *Tilton et al*., 1981] and exposed in a series of massifs within the Oman Mountains. The dated samples were collected in the Wadi Tayin, Samail, Rustaq, Haylayn, and Fizh massifs (Figure 1), which each expose large sections of crust and mantle. The general crustal stratigraphy in each massif, starting at the crust-mantle boundary, consists of layered gabbro (1–4 km); foliated gabbro (0.3–2 km); upper level gabbro and tonalite, trondhjemite, and quartz diorite (<1 km); and sheeted dikes and basaltic pillows and lavas (1.5–2 km; thicknesses from *Coogan et al*. [2002b] and *Nicolas et al*. [1996]). This sequence is locally intruded by younger magmatic series that include pyroxenites, gabbronorites, olivine gabbros, and wehrlites. These late intrusions are more abundant in the northern massifs (Rustaq massif and north), where they are likely related to multiple volcanic series [*Adachi and Miyashita*, 2003; *Alabaster et al*., 1982; *Boudier et al*., 2000; *Goodenough et al*., 2010; *Juteau et al*., 1988a; *Juteau et al*., 1988b; *Pearce et al*., 1981; *Python and Ceuleneer*, 2003; *Smewing*, 1981; *Tamura and Arai*, 2006]. In the southern massifs (Samail and Wadi Tayin), gabbronorites and pyroxenites are limited to minor intrusions in the mantle [*Amri et al*., 1996; *Benoit et al*., 1996; *Hanghøj et al*., 2010; *Kelemen et al*., 1997b; *Python and Ceuleneer*, 2003].

[5] The extrusive volcanic record has been divided into five main units based on stratigraphy and geochemistry: Geotimes, Alley, Lasail, clinopyroxene-phyric, and Salahi [*Alabaster et al*., 1982; *Pearce et al*., 1981]. The Geotimes unit directly overlies, and is intruded by, the sheeted dike complexes in all of the ophiolite massifs and is generally interpreted as the extrusive complement to the gabbroic crust and sheeted dikes [e.g., *Ernewein et al*., 1988]. The compositions of these lavas are the most similar to mid-ocean ridge basalt (MORB) [*Alabaster et al*., 1982; *Ernewein et al*., 1988; *Godard et al*., 2003; *Godard et al*., 2006; *Pallister and Knight*, 1981; *Pearce et al*., 1981], although their fractionation trend extends to lower Ti and higher SiO_2 contents than typical MORB [*MacLeod et al*., 2013]. The Alley, Lasail, and clinopyroxene-phyric units overlie the Geotimes lavas north of the Haylayn massif. These series generally have lower Ti, rare earth element (REE), and high field strength element (HFSE) concentrations [*Alabaster et al*., 1982; *Ernewein et al*., 1988; *Godard et al*., 2003; *Pearce et al*., 1981] and can be attributed to subduction related volcanism [*Pearce et al*., 1981] and/or melting of a previously depleted mantle [*Ernewein et al*., 1988; *Godard et al*., 2003]. Lavas with boninitic compositions, which are often attributed to subduction initiation in arc settings, have been identified in the Alley lavas [*Ishikawa et al*., 2002]. The Salahi lavas are separated from the underlying units by a relatively thick (~15 m) layer of pelagic sedimentary rocks and are thought to post-date formation of the ophiolite crust [*Ernewein et al*., 1988]. *Ernewein et al*. [1988] proposed a simplified nomenclature in which the Geotimes unit is labeled V1; the Lasail, Alley, and clinopyroxene-phyric units are condensed into a single V2 unit; and the Salahi unit is labeled V3. For simplicity, we adopt the *Ernewein et al*. [1988] nomenclature, recognizing that the V2 unit includes a progression from the Lasail through Alley and/or clinopyroxene-phyric lavas. For a discussion of different interpretations of the lava stratigraphy, see *Kusano et al*. [2012].

[6] A thin metamorphic sole is preserved in several localities along the margin of the ophiolite or in tectonic widows within it [*Nicolas et al*., 2000; *Searle and Malpas*, 1980]. The sole preserves an inverted metamorphic gradient [*Searle and Malpas*, 1980] with peak P-T conditions of ~840–870°C and 11–14 kbar [*Gnos*, 1998; *Searle and Cox*, 2002]. Most of the exposed sole consists of amphibolite grade or lower metabasalts, marbles, quartzites, and volcanoclastic rocks [*Cox et al*., 1999; *Searle and Cox*, 2002]. However, in the Bani Halid area in the UAE, the sole exposures include granulite facies enstatite-cordierite-sillimanite-spinel ± sapphirine quartzites, alkaline mafic granulites, and calc silicates [*Cox et al*., 1999; *Gnos and Kurz*, 1994; *Searle and Cox*, 1999]. In the Wadi Sumeini and Wadi Tayin exposures, small trondhjemitic, tonalitic, and monzodioritic pods are interpreted as leucocratic melts of sole amphibolites [*Searle and Cox*, 2002; *Searle and Malpas*, 1982; *Warren et al*., 2005]. A thrust fault below the metamorphic sole separates the metamorphic rocks from lower-grade sedimentary and volcanic rocks of the Haybi and Hawasina complexes in several of the sole exposures [*Searle and Malpas*, 1980; *Searle et al*., 1980].

[7] Most of the samples dated in this study come from upper level gabbros, tonalites, trondhjemites, and quartz diorites, which are exposed just below the sheeted dikes (Figures 1b–1d; Table 1), intruding into the dikes in some localities. These rocks types are generally interpreted as either residual liquids derived from fractionation of mantle derived magmas [*Amri et al*., 1996; *France et al*., 2009; *Kelemen et al*., 1997a; *MacLeod and Yaouancq*, 2000; *Pallister and Hopson*, 1981; *Tilton et al*., 1981] or melts related to interaction between the magmatic and hydrothermal systems [*Koepke et al*., 2004; *Nicolas and Boudier*, 2011;

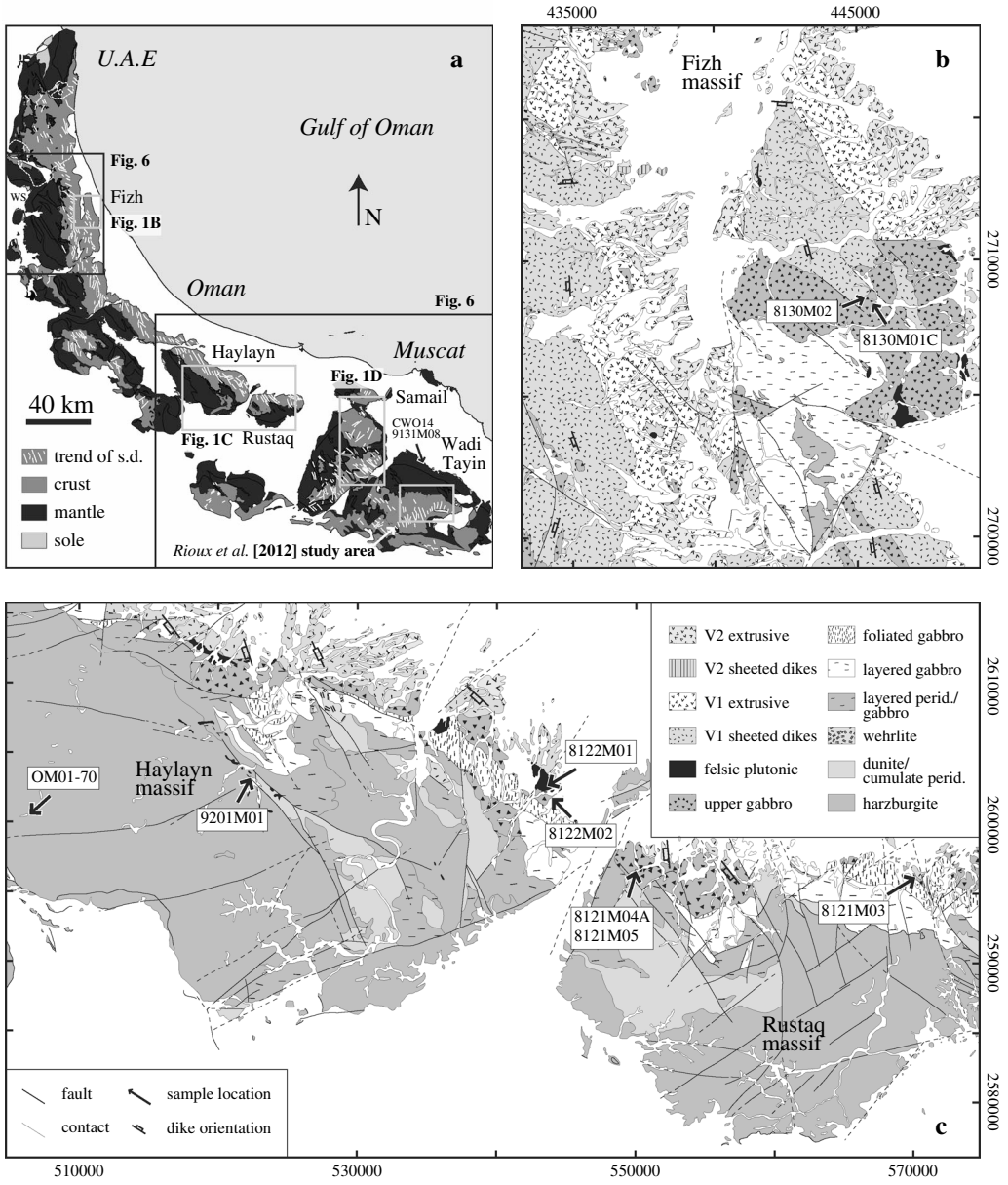

Figure 1. Geologic maps of the Samail ophiolite. (a) Location map [modified from *Nicolas et al*., 2000]. White solid lines show sheeted dike (s.d.) orientations, and white dashed lines are the Oman-United Arab Emirates (UAE) borders. The locations of samples CWO14 and 9131M08 are plotted at the edge of the Wadi Tayin massif. WS marks Wadi Sumeini. Gray rectangles show the locations of Figures 1b–1d and the study area of *Rioux et al*. [2012a], and black rectangles show the locations enlarged in Figure 6. (b–d) Geologic maps of the study areas outlined on the location map [modified from *Beurrier et al*., 1986a, 1986b; *Bishimetal Exploration Co*. *Ltd*., 1987; *Chévremont et al*., 1993; *Rabu et al*., 1986; *Villey et al*., 1986]. Map keys are provided in Figure 1c. Sample locations are shown with arrows. The "wehrlite" unit includes wehrlite, troctolite, plagioclase-bearing dunite, and olivine clinopyroxenite. Numbers along the axes are UTM coordinates. Representative sheeted dike orientations are shown with the tick in the down dip direction.

Nicolas et al., 2008; *Rollinson*, 2009; *Stakes and Taylor*, 2003] (see *Rioux et al*. [2012a] for a more detailed discussion).

[8] A subset of the dated tonalites and trondhjemites is from deeper sills, dikes, and stocks that intrude layered gabbro and mantle harzburgite. Published isotopic analyses of granites, granodiorites, tonalites, and trondhjemites that intrude the mantle generally have lower $\varepsilon_{Nd}(t)$ (−6.3 to +7.8) [*Amri et al*., 2007; *Cox et al*., 1999] than the gabbros, tonalites, trondhjemites, and basalts that make up most of the ophiolite crust (+7.5 to +8.8) [*Amri et al*., 2007; *Godard et al*., 2006; *McCulloch et al*., 1981; *Rioux et al*., 2012a]. The intrusions within the mantle are also typically enriched in light rare earth elements (LREE) and fluid mobile trace elements relative to MORB [*Amri et al*., 2007; *Briqueu et al*., 1991; *Cox et al*.,

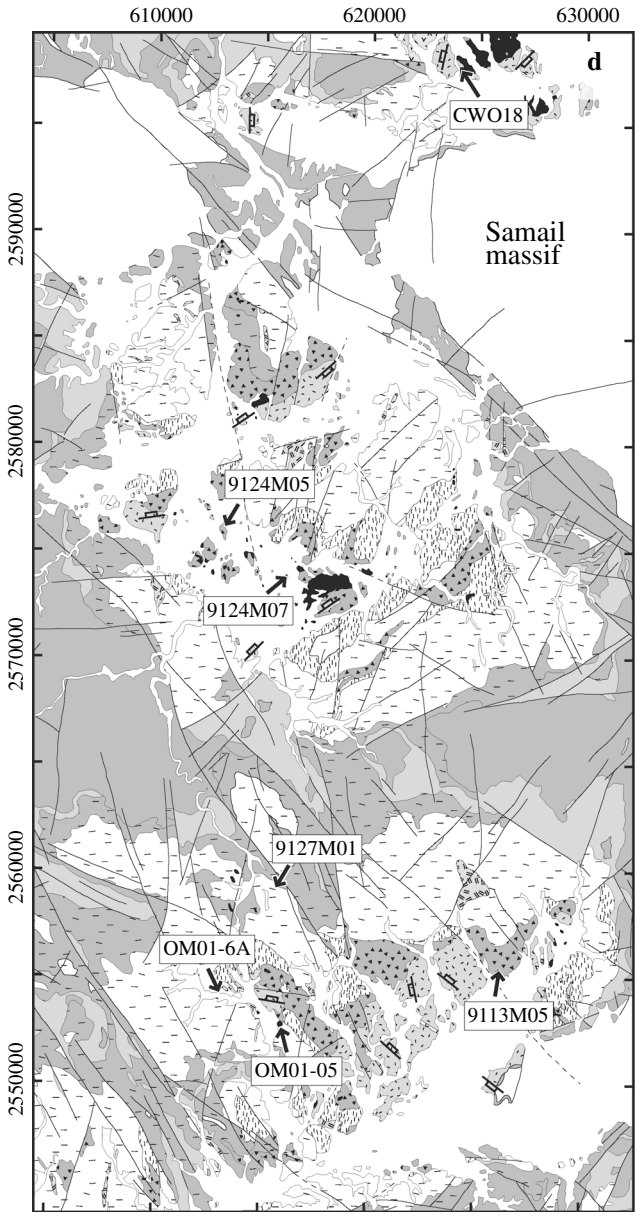

Figure 1. (Continued)

1999; *Rollinson*, 2009]. The distinct isotopic and trace element signatures have been attributed to melting or assimilation of rocks in the metamorphic sole, the underlying Haybi complex, and/or other rocks subducted/thrust under the ophiolite [*Amri et al*., 2007; *Briqueu et al*., 1991; *Cox et al*., 1999; *Lippard et al*., 1986; *Rollinson*, 2009]. Two additional trondhjemite samples from this study are from the metamorphic sole of the ophiolite in the Wadi Tayin massif and are interpreted as partial melts of nearby amphibolites (Figure 1a) [*Warren et al*., 2005].

3. Existing Geochronology

[9] Prior to *Rioux et al*. [2012a] and this study, three published studies used U-Pb zircon dating to determine the crystallization ages of plutonic rocks within the ophiolite. To compare the dates from these studies with those presented here, the dates reported herein are Th-corrected, as described in *Rioux et al.* [2012a]. *Tilton et al*. [1981] and *Warren et al*. [2005] primarily focused on tonalites and trondhjemites from throughout the ophiolite massifs in Oman and reported $^{206}Pb/^{238}U$ dates on multi-grain fractions of 97.3 ± 0.4 to 93.5 ± 0.4 Ma (Th-corrected). *Warren et al*. [2005] also dated an amphibolite and a trondhjemite pod from the metamorphic sole, interpreted as a partial melt, and reported $^{206}Pb/^{238}U$ dates on small multi-grain fractions of 96.28 ± 0.27 to 93.61 ± 0.24 Ma (Th-corrected). Finally, *Goodenough et al*. [2010] dated two gabbroic pegmatites and the felsic phase of a mingled-magma intrusion from the ophiolite massifs in the UAE and reported $^{206}Pb/^{238}U$ dates on small multi-grain fractions of 95.76 ± 0.48 to 95.22 ± 0.37 Ma (uncorrected).

[10] In *Rioux et al*. [2012a], we reported single grain and grain fragment U-Pb zircon dates from 12 samples from a well preserved and exposed crustal section from the center of the Wadi Tayin massif. The dated samples were collected along a ~30 km transect perpendicular to the sheeted dike trend. Eight upper level gabbros, one trondhjemite, one tonalite, and one gabbroic pegmatite yielded single grain and grain fragment Th-corrected $^{206}Pb/^{238}U$ dates that ranged from 99.15 ± 0.10 to 95.50 ± 0.17 Ma, with most data clustered between 96.40 ± 0.17 to 95.50 ± 0.17 Ma. Three upper level gabbros (8112M04, 8112M06, 8112M07A) had >1 Ma intra-sample variability in single grain dates, which we attributed to assimilation of older crust into ridge magmas as a result of ridge propagation. Whole rock Nd isotopic data from six of the dated gabbros, a dated trondhjemite and a single undated gabbro ranged from 7.59 ± 0.23 to 8.28 ± 0.31, similar to other ridge-related plutonic and volcanic rocks in the ophiolite [*Benoit et al*., 1996; *Godard et al*., 2006; *McCulloch et al*., 1981; *Rioux et al*., 2012a] and mid-ocean ridge basalts from the Atlantic and Indian Oceans [e.g., *Hofmann*, 2003]. A single gabbroic pegmatite from the base of the crust (8111M02, 9114M01A) had a surprisingly large range in $^{206}Pb/^{238}U$ dates of 95.78 ± 0.10 to 112.55 ± 0.21 Ma, and further work is needed to understand the origin of this intrusion and the >100 Ma xenocrystic zircons.

[11] In addition to U-Pb geochronology, K-Ar and ^{40}Ar-^{39}Ar geochronology has provided important insights into the thermal history of the ophiolite and metamorphic sole [*Gnos and Peters*, 1993; *Hacker*, 1994; *Hacker et al*., 1996; *Lanphere*, 1981; *Montigny et al*., 1988; *Searle et al*., 1980]. A comprehensive study by Hacker et al. [*Hacker*, 1994; *Hacker et al*., 1996] demonstrated that $^{40}Ar/^{39}Ar$ hornblende cooling dates for crustal plutonic rocks (98.4 ± 2.6 to 95.3 ± 1.0 Ma) and metamorphic rocks in the sole (93.3 ± 1.0 to 94.6 ± 1.2 Ma) overlap within uncertainty, implying rapid development of the emplacement thrust following formation of the ophiolite crust ($\pm 2\sigma$ analytical + standard; reported dates are re-calculated as described in *Rioux et al*. [2012a]).

4. Results

[12] U-Pb zircon data are reported in Table S1 and plotted in Figure 2. Single grain and grain fragments were analyzed by isotope dilution-thermal ionization mass spectrometry

Table 1. Sample Locations and Descritions

Sample	UTM (E)[a]	UTM (N)[a]	Massif	Rock Type	Mineralogy[b]
8121M03	0570077	2596918	Rustaq	gabbro	pl+cp+ox+(am)
8121M04A	0550020	2596577	Rustaq	trondhjemite	pl+qt+ox
8121M05	0549997	2596551	Rustaq	gabbro	pl+cp+(am)
8122M01	0543647	2602683	Haylayn	tonalite	pl+qt+am+ox
8122M02	0544056	2601807	Haylayn	gabbronorite	pl+cp+op+ox+(am)
8130M01C	0445627	2708335	Fizh	gabbro	pl+am+ox
8130M02	0445406	2708416	Fizh	tonalite	pl+qt+am+ox
9113M05	0626184	2555253	Samail	gabbro	pl+am+ox
9124M05	0613362	2576316	Samail	gabbro	pl+am+ox
9124M07	0616232	2573782	Samail	tonalite	pl+qt+am+ox
9127M01	0615805	2559221	Samail	tonalite	pl+qt+am+ox
9131M08	0663975	2550903	Wadi Tayin	trondhjemite	
9201M01	0522346	2603179	Haylayn	trondhjemite	pl+qt+ox
CWO14[c]	0663971	2550936	Wadi Tayin	trondhjemite	pl+qt+kf+ms
CWO18[c]	0623929	2597795	Samail	tonalite	pl+qt+am
OM01-05	0616069	2552941	Samail	tonalite	
OM01-6A	0613086	2554258	Samail	gabbro	pl+am+ox
OM01-70	0506458	2600564	Haylayn	granite	pl+qt+kf+bt+ms+ox

[a]WGS 84, zone 40.
[b]am, amphibole; bt, biotite; cp, clinopyroxene; kf, K-feldspar; ms, muscovite; op, orthopyroxene; ox, oxide; pl, plagioclase; qt, quartz; parentheses denote secondary minerals.
[c]Mineralogy from *Warren et al*. [2005].

(ID-TIMS) using the chemical abrasion method [*Mattinson*, 2005], following the procedures described in *Rioux et al*. [2012a]. The data can be divided into four groups based on the observed range of dates in each sample, consistent with the data descriptions in *Rioux et al*. [2012a]. Individual analyses with $^{206}Pb/^{238}U$ 2σ uncertainties ≥ 0.5 Ma are excluded from all figures and the discussion of the data for clarity. All of the lower precision analyses overlap within uncertainty with higher precision dates but have low radiogenic Pb to common Pb ratios ($Pb^*/Pbc < 2.5$) relative to the other data from this study, as a result of either low total Pb* and/or slightly elevated analytical blanks. The low Pb* analyses included small and/or low U zircons and high U metamic zircons that were heavily leached during the chemical abrasion procedure. All of the dates in the figures and text are $^{206}Pb/^{238}U$ dates that have been corrected for initial exclusion of ^{230}Th from the ^{238}U decay chain [*Rioux et al*., 2012a; *Rioux et al*., 2012b]. Reported intra-sample ranges in dates were calculated as the difference between the maximum and minimum dates in each sample with uncertainties equal to the sum of the uncertainties of these dates.

[13] Group I: Three gabbros (8121M05, 8130M01C, 9124M05) and five tonalites/trondhjemites (8121M04A, 8122M01 9124M07, 9201M01, CWO18) yielded single grain $^{206}Pb/^{238}U$ dates within each sample that overlap within uncertainty. The mean square of the weighted deviates (MSWD) of the weighted mean date for each sample (all ≤ 2.1) are consistent with the null hypothesis that the data represent repeat measurements of a single population. The single grain $^{206}Pb/^{238}U$ dates range from 95.91 ± 0.48 to 95.16 ± 0.23 Ma. An additional tonalite (8130M02) yielded a cluster of four overlapping single grain $^{206}Pb/^{238}U$ dates of 95.58 ± 0.41 to 95.17 ± 0.16 Ma (MSWD = 2.0) and a single outlying younger date of 94.30 ± 0.18 Ma. We interpret the younger date to be a product of minor residual Pb loss and the cluster of dates as the best estimate of the crystallization age.

[14] Group II: One gabbronorite (8122M02) and two tonalites (OM01-05, 9127M01) yielded a single cluster of $^{206}Pb/^{238}U$ dates with no clear outliers but weighted mean MSWDs that are higher than expected for repeat measurements of a single population (MSWD ≥ 3.4; two-sided *p*-values for the chi-squared goodness of fit of < 0.05). The single grain $^{206}Pb/^{238}U$ dates range from 95.61 ± 0.06 to 95.08 ± 0.06 Ma. The spread in dates in the three samples range from 0.13 ± 0.11 to 0.29 ± 0.12 Ma.

[15] Group III: An upper level gabbro (9113M05) and a gabbroic pegmatite (OM01-6A) yielded a cluster of $^{206}Pb/^{238}U$ dates and a single <1 Ma older outlying data point. In 9113M05, the younger single grain dates all overlap within uncertainty and fall between 96.00 ± 0.05 to 95.93 ± 0.08 Ma, and the older outlier has a date of 96.28 ± 0.05 Ma; the total range of dates is 0.35 ± 0.14 Ma. In OM01-6A, the younger dates are slightly more dispersed and range from 96.14 ± 0.22 to 95.69 ± 0.17 Ma, and the older outlier has a date of 96.44 ± 0.06 Ma; the entire range of dates is 0.75 ± 0.23 Ma and comes from multiple fragments of a single grain (z1b–z1d).

[16] Group IV: A trondhjemite (CWO14) from the metamorphic sole and a granitic dike (OM01-70) that intrudes mantle harzburgites generated $^{206}Pb/^{238}U$ dates that span >10 Ma. CWO14 yielded three younger $^{206}Pb/^{238}U$ dates from 94.90 ± 0.38 to 94.69 ± 0.12 Ma and a single concordant older date of 170.29 ± 0.24 Ma (the older date plots off-scale in Figures 2). We interpret the younger dates as the best estimate of the crystallization age of the melt and the older date to be an inherited xenocryst. OM01-70 yielded a single younger date of 77.22 ± 0.65 Ma and a group of older dates that range from 95.24 ± 0.43 to 93.74 ± 0.18 Ma. We interpret the youngest date as the maximum crystallization age for the dike and the older dates as either mixed ages of cryptic xenocrystic cores with younger rims, or as ages of whole xenocrystic grains.

Table 2. Whole Rock Sm-Nd Isotope Data

	Sm[a]	± 2σ	Nd[a]	± 2σ	$^{147}Sm/^{144}Nd$[b]	± 2σ	$^{143}Nd/^{144}Nd$[b]	± 2σ	$^{143}Nd/^{144}Nd_{96\ Ma}$[b]	± 2σ	$\varepsilon_{Nd}(0)$[c]	± 2σ	$\varepsilon_{Nd}(96)$[c]	± 2σ
8121M05	0.938	0.005	2.161	0.011	0.2624	0.0022	0.513132	0.000010	0.512967	0.000010	9.64	0.20	8.83	0.20
8130M01C	1.082	0.006	3.050	0.015	0.2145	0.0018	0.513053	0.000008	0.512918	0.000008	8.10	0.16	7.88	0.16
8130M02	1.820	0.010	5.034	0.025	0.2186	0.0018	0.513035	0.000008	0.512898	0.000008	7.74	0.15	7.48	0.16
9124M05	1.124	0.006	3.771	0.018	0.1802	0.0016	0.512996	0.000006	0.512883	0.000006	6.98	0.12	7.19	0.12
9124M07	1.543	0.008	5.646	0.028	0.1652	0.0014	0.512990	0.000008	0.512886	0.000008	6.87	0.16	7.25	0.16
9127M01	1.519	0.008	3.828	0.019	0.2400	0.0020	0.513019	0.000006	0.512868	0.000006	7.43	0.12	6.90	0.12
9131M08	1.677	0.009	4.430	0.022	0.2400	0.0020	0.512306	0.000008	0.512155	0.000008	−6.48	0.16	−7.01	0.16
9201M01	2.108	0.011	12.897	0.063	0.2400	0.0008	0.512267	0.000004	0.512116	0.000004	−7.24	0.08	−7.77	0.08

[a]Sm and Nd concentrations (ppm) determined by isotope dilution. All reported uncertainties are 2σ absolute.
[b]Fractionation, blank, and spike corrected isotopic ratios. Initial ratios are corrected to 96 Ma.
[c]ε_{Nd} values calculated for 0 and 96 Ma using present day bulk Earth value of $^{143}Nd/^{144}Nd = 0.512638$ and $^{147}Sm/^{144}Nd = 0.1967$ and ^{147}Sm decay constant of $6.54 \times 10^{-12}\ yr^{-1}$.

[17] Two of the dated samples (CWO14 and CWO18) were collected and previously dated by *Warren et al*. [2005] using ID-TIMS on multi-grain fractions ($n = 3$–48 grains). *Warren et al*. [2005] dated the samples prior to the widespread adoption of the chemical abrasion method [*Mattinson*, 2005], and the data are therefore more likely to be affected by post-crystallization Pb loss. For CWO14, *Warren et al*. [2005] analyzed five fractions that yielded $^{206}Pb/^{238}U$ dates of 96.28 ± 0.27 to 93.67 ± 0.13 Ma. These dates are comparable to the cluster of younger dates in our analyses (94.90 ± 0.38 to 94.69 ± 0.12 Ma) but stretch to both younger and older values. Our single grain analyses demonstrate that this sample contains xenocrystic zircons and the one significantly older fraction from Warren et al. ($n = 38$ grains) may include one or more xenocrystic cores/grains. The two younger fractions ($n = 9$ and 48 grains) may be affected by Pb loss. For CWO18, *Warren et al*. [2005] analyzed three fractions ($n = 3$–5) that yielded a cluster of $^{206}Pb/^{238}U$ dates from 94.44 ± 0.24 to 94.18 ± 0.54 Ma. The dates are significantly younger than our single grain dates from this sample (95.36 ± 0.27 and 95.67 ± 0.48 Ma), and all other dated rocks from this study and *Rioux et al*. [2012a], and again we speculate that this is attributable to Pb loss.

[18] Five of the dated samples (8121M04A, 8121M05, 8122M01, 8122M02, and CWO18) were collected from the same location or close to three of the *Tilton et al*. [1981] sample locations (H618, H619, P700). *Tilton et al*. [1981] dated large multi-grain fractions (~10 mg), and the grains were not physically or chemically abraded prior to analysis. In each location, the Tilton et al. $^{206}Pb/^{238}U$ dates are slightly younger than the new dates we report here. For location H618, the old and new dates agree within uncertainty, while at locations H619 and P700, the old dates are 0.3–1.2 Ma younger. We attribute the offset to Pb loss in the zircon aliquots dated by *Tilton et al*. [1981] and/or inter-laboratory bias related to the calibration of the U-Pb tracers used in the two studies.

[19] We analyzed whole rock Sm-Nd isotopes by ID-TIMS from seven of the dated gabbros, tonalites, and trondhjemites from the crust and upper mantle, and a trondhjemite from the same exposure of the metamorphic sole as CWO14 (Figure 3; Table 2). Analytical procedures are described in *Rioux et al*. [2012a]. Six gabbro and tonalite samples (8121M05, 8130M01C, 8130M02, 9124M05, 9124M07, and 9127M01) had $\varepsilon_{Nd}(96\ Ma) = 6.90 \pm 0.12$ to 8.83 ± 0.20. A trondhjemite dike from the upper mantle (9201M01) and the small trondhjemite pod from the metamorphic sole (9131M08) had $\varepsilon_{Nd}(96\ Ma) = -7.77 \pm 0.08$ and -7.01 ± 0.16, respectively.

5. Discussion

5.1. Interpretation of the U-Pb Dates

[20] As in *Rioux et al*. [2012a], we interpret the youngest cluster of dates in each sample as the best estimate for the crystallization ages of the rocks, and the intra-sample variability in single grain and grain fragment dates in the Group II (0.13 ± 0.11 to 0.29 ± 0.12 Ma) samples as a result of either protracted zircon crystallization in a magma chamber or mush zone and/or assimilation of zircons from adjacent wall rocks. For the Group III and IV samples, we consider it most likely that the outlying older dates are from xenocrystic zircons that were assimilated into younger magmas. The wide range of dates from fragments of a single grain from sample OM01-6A (0.75 ± 0.23 Ma) are consistent with the presence of an older xenocrystic core surrounded by a younger rim.

5.2. Tectonic Setting During On-Axis Crustal Growth

[21] The rocks analyzed in this study can be broadly divided into two groups based on their structural position, dates, and isotopic composition (Figures 4 and 5): an older group related to on-axis magmatism ($^{206}Pb/^{238}U > 95.4$ Ma) and a younger group of post-ridge dikes, sills, and stocks ($^{206}Pb/^{238}U < 95.4$ Ma). In this section, we discuss the on-axis samples and their implications for the tectonic setting during the formation of the ophiolite crust, in the context of the different ophiolite massifs. The dated on-axis samples consist of upper level gabbros and tonalites from between the foliated gabbros and the sheeted dikes.

5.2.1. Samail Massif

[22] The Samail massif can be divided into three distinct domains based on systematic changes in sheeted dike orientations: dikes in the center of the massif are oriented NW-SE, while dikes in northeast and southwest portions of the massif are oriented NE-SW, although there is some variability in the latter areas (Figures 1a, 1c, and 6) [*MacLeod and Rothery*, 1992; *Nicolas et al*., 2000]. The change in orientations has been attributed to a younger NW-SE trending ridge propagating into older crust formed at a NE-SW trending ridge (Figure 6; current azimuths) [e.g., *Boudier et al*., 1997].

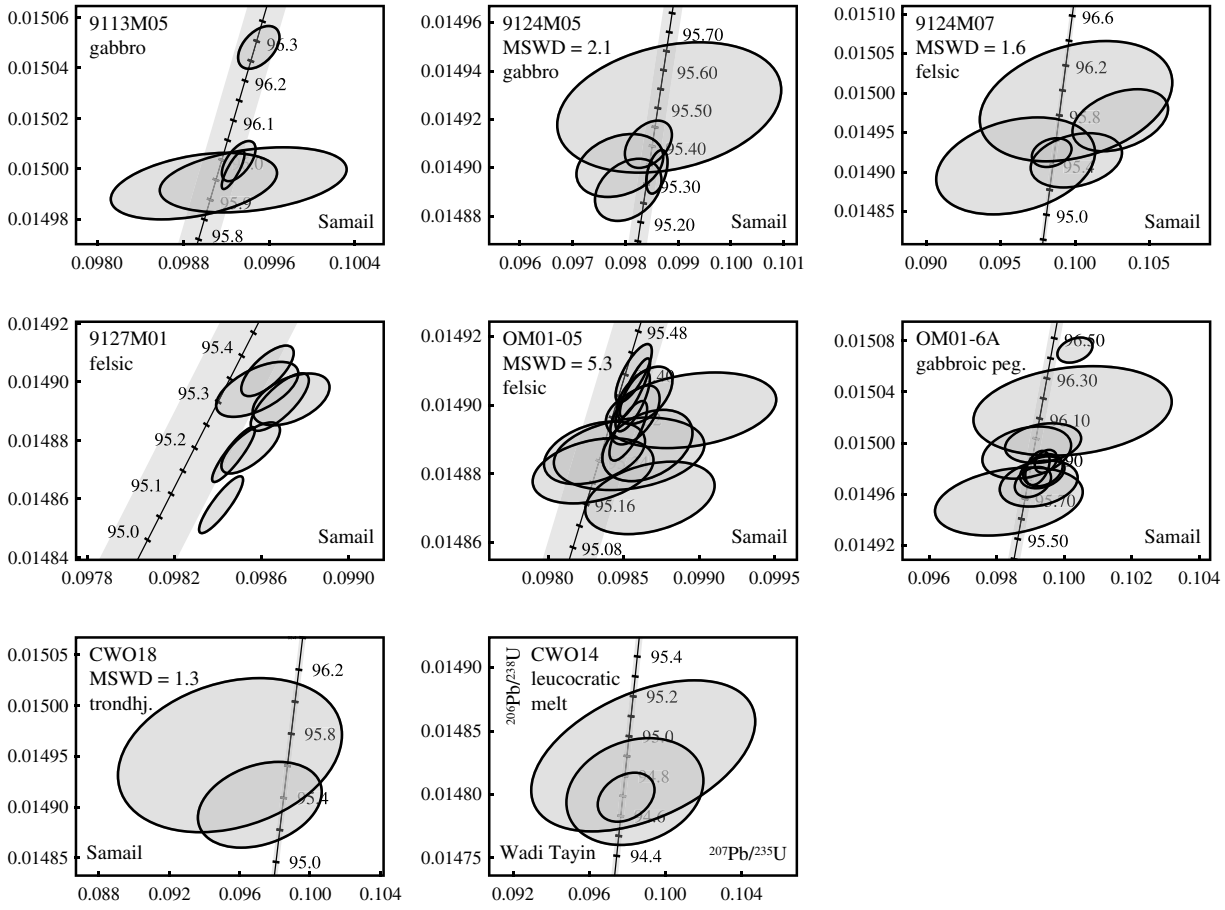

Figure 2. U-Pb concordia diagrams of single-grain and grain fragment zircon dates. All data are corrected for initial Th exclusion. Ages on concordia are in Ma. Gray bands represent 2σ uncertainties on concordia based on decay constant uncertainties of 0.107% (^{238}U) and 0.136% (^{235}U) [*Jaffey et al*., 1971]. Axis labels are shown in plots on lower right, and the massif locations are listed in each plot. Plots and mean square of the weighted deviates (MSWD) of the weighted mean were generated using the U-Pb_redux software package [*Bowring et al*., 2011; *McLean et al*., 2011]. Analyses with $^{206}Pb/^{238}U$ 2σ uncertainties >0.5 Ma were excluded for clarity.

[23] We dated two on-axis samples from the center of the massif: an upper level gabbro that is cut by NW-SE oriented dikes (9113M05) and a centimeter-scale gabbroic pegmatite dike that cuts layered gabbro (OM01-6A) (Figure 1d). These samples have $^{206}Pb/^{238}U$ dates of 96.441 ± 0.062 to 95.69 ± 0.17 Ma, which overlap dates from the Wadi Tayin massif that we reported in *Rioux et al*. [2012a]. Sheeted dike trends in the Wadi Tayin massif and the center of the Samail massif are similar, although there is a systematic rotation in the dike trends within the Wadi Tayin massif, and the coeval dates indicate that the two areas either formed at a single ridge or two coeval, parallel ridges. The relatively large range of dates in the Samail samples (0.35 ± 0.14 Ma and 0.75 ± 0.23 Ma) is also similar to, although less extreme than, the evidence for xenocrystic zircons in some of the Wadi Tayin gabbros [*Rioux et al*., 2012a].

5.2.2. Rustaq and Haylayn Massifs

[24] As in the Samail massif, structural relationships in the Rustaq and Haylayn massifs are consistent with propagation of younger ridge segments into older oceanic lithosphere. In the central part of the Rustaq massif, thinned or nonexistent gabbroic crust and sheeted dikes that root directly into peridotite have been interpreted as the preserved tip of a northward propagating ridge [*Nicolas and Boudier*, 1995]. In the southeastern part of the Haylayn massif, a rotation in the sheeted dike orientation, two generations of dikes with N-S and NW-SE orientations and a large volume of laminated gabbronorite have been attributed to both southward and northward ridge propagation [*MacLeod and Rothery*, 1992; *Reuber et al*., 1991].

[25] In the Rustaq massif, we dated three samples: an upper level gabbro and adjacent trondhjemite from the western end of the massif (8121M04A, 8121M05) and an upper level gabbro from the mouth of Wadi Abyad (8121M03), a well-studied crustal section in the center of the massif (Figure 1c) [*Browning*, 1984; *Coogan et al*., 2002a; *Coogan et al*., 2002b; *Korenaga and Kelemen*, 1997; *Korenaga and Kelemen*, 1998; *MacLeod and Yaouancq*, 2000; *Nicolas and Boudier*, 1995]. In the Haylayn massif, we dated an upper level gabbronorite and an adjacent tonalite from the southeastern corner of the massif (8122M01, 8122M02) (Figure 1c). The gabbro from Wadi Abyad yielded the oldest dates with the most precise results defining a tight cluster of $^{206}Pb/^{238}U$ dates between 96.16 ± 0.12 and 96.095 ± 0.071 Ma. The four

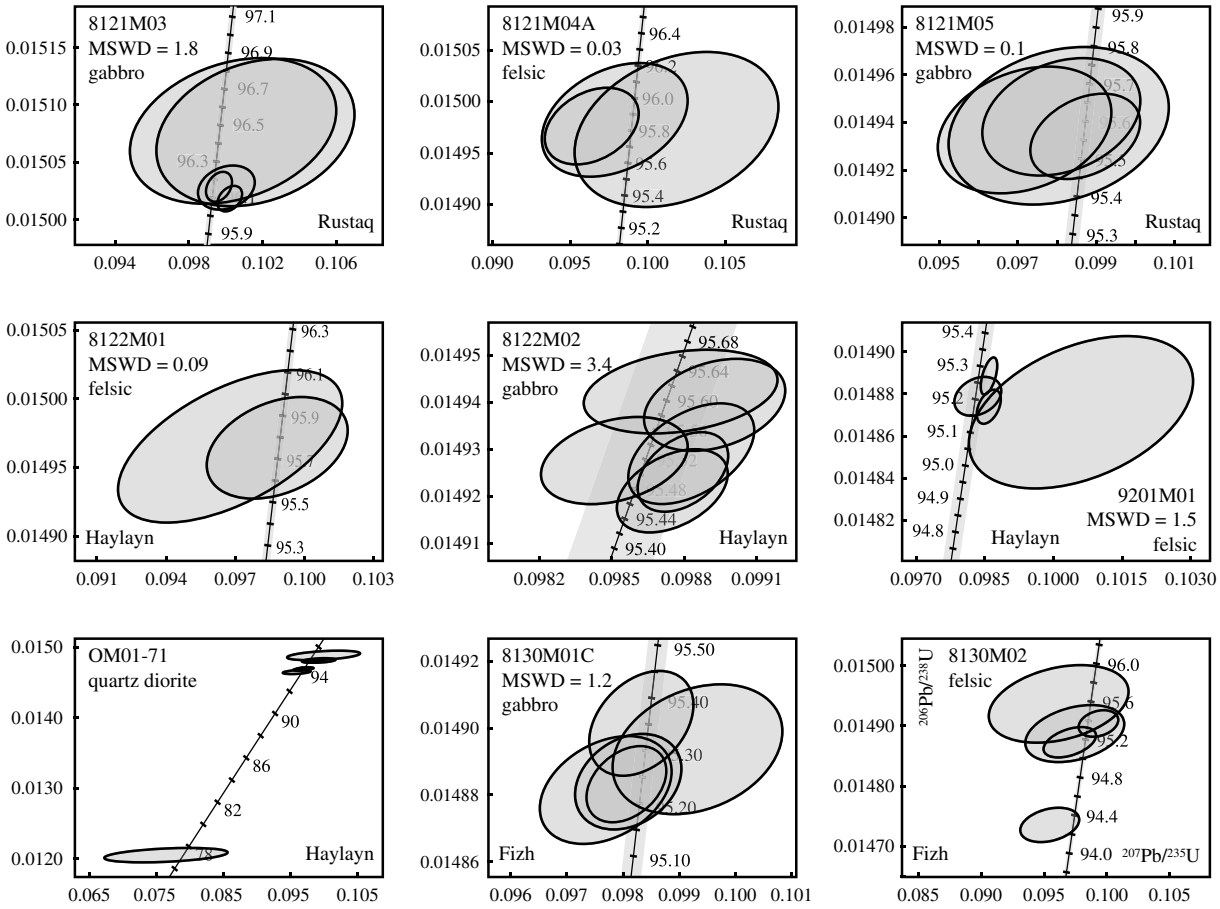

Figure 2. (Continued)

other samples from the Rustaq and Haylayn massifs yielded younger dates that all overlap within uncertainty: the two gabbros have $^{206}Pb/^{238}U$ dates between 95.612 ± 0.0156 and 95.478 ± 0.056 Ma, and the most precise analyses from the two tonalites have $^{206}Pb/^{238}U$ dates between 95.87 ± 0.35 and 95.75 ± 0.24 Ma. The younger gabbro from the Rustaq massif (8121M05) has $\varepsilon_{Nd}(96\ Ma) = 8.83 \pm 0.20$, consistent with published data from the main phase of the ophiolite crust (Figure 3). These data support the previously recognized evidence for ridge propagation in this area, with the Wadi Abyad section representing slightly older oceanic lithosphere and the rocks in the western Rustaq massif and southeastern Haylayn massif being related to younger magmatism (Figure 6). The offset between the older lithosphere and younger ridge is ~0.5 Ma. The overlap between the younger dates in both massifs is consistent with formation at either a single ridge or overlapping (en-echelon) ridge segments [*Nicolas et al.*, 2000].

[26] The field evidence for propagating ridges and the similar orientations of sheeted dikes in both the Rustaq and Samail massifs could be interpreted as evidence that the crust in both massifs formed at a single northwestward propagating NW-SE oriented ridge. However, the dated gabbros in the Rustaq and Haylayn massifs are 0.25–0.5 Ma younger than gabbros in the center of the Samail massif, suggesting that the Rustaq and Haylayn gabbros formed at a younger ridge than the Samail gabbros (see *Boudier et al.* [1997] and *Nicolas et al.* [2000] for models that incorporate multiple propagating ridges within the Samail and Rustaq massifs).

5.2.3. Summary

[27] The combined dataset from this study and *Rioux et al.* [2012a] record on-axis magmatism in the Wadi Tayin, Samail, Rustaq, and Haylayn massifs from ~96.25–95.5 Ma. Initial Nd data from samples attributed to on-axis magmatism from the two studies include nine gabbros, tonalites, and trondhjemites, which all have Nd isotopic ratios that are similar to modern mid-ocean ridges, suggesting the parental magmas were generated by partial melting of an Indian or Atlantic type MORB mantle source (Pb isotopes from the Oman volcanic rocks are more similar to Indian Ocean MORB [*Godard et al.*, 2006]). The two generations of gabbro within the Rustaq massif and the evidence for xenocrystic zircons in the Samail massif are consistent with the evidence for xenocrystic zircons in the Wadi Tayin massif [*Rioux et al.*, 2012a], which we attributed to the propagation of a younger ridge into older oceanic lithosphere. Taken together, the data suggest that the ophiolite crust formed in a dynamic tectonic environment where there were multiple ridge segments propagating into older oceanic lithosphere.

5.3. Post-Ridge Magmatism

[28] The studied post-ridge dikes, sills, and stocks intrude all levels of the crust, the upper mantle, and the metamorphic sole. These rocks generally have $^{206}Pb/^{238}U$ dates < 95.4 Ma;

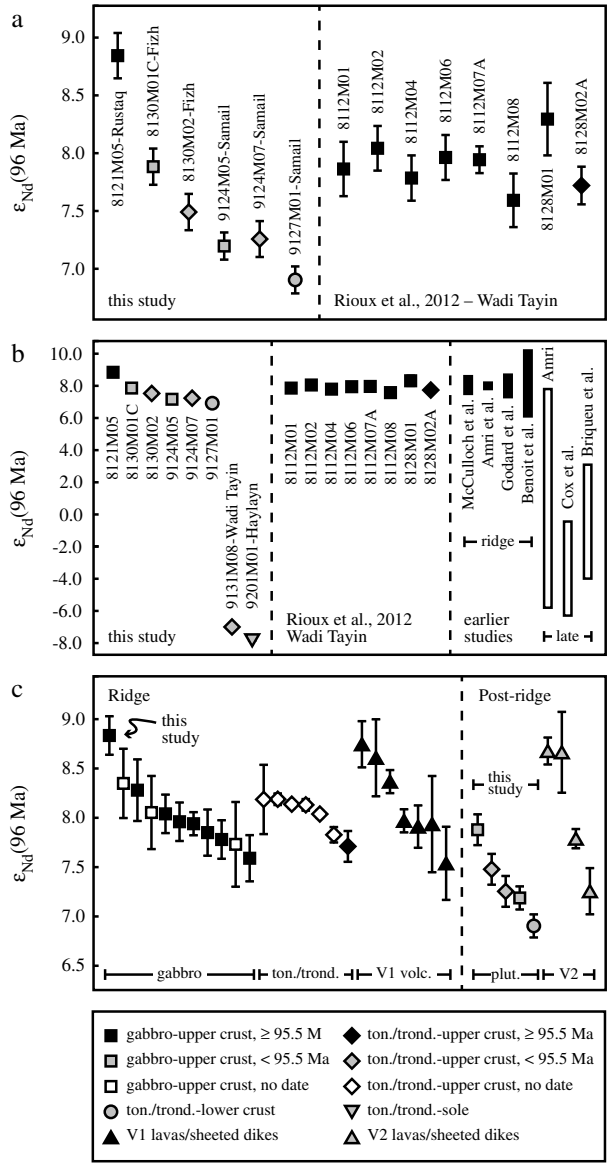

Figure 3. ε_{Nd}(96 Ma) for samples from this study, *Rioux et al*. [2012a], and previous work. (a) Data from samples with $\varepsilon_{Nd}(96\ Ma) > 6.5$ from this study and *Rioux et al*. [2012a]. (b) Data from all samples. Uncertainties are smaller than the data points. The range of ε_{Nd}(96 Ma) for published data is separated into rocks attributed to ridge magmatism (black) and late dikes and sills in the mantle (open). Published data are from *McCulloch et al*. [1981], *Benoit et al*. [1996], *Godard et al*. (V1 only) [2006], *Amri et al*. [2007], *Cox et al*. [1999], and *Briqueu et al*. [1991]. (c) ε_{Nd}(96 Ma) for samples from the crust. Data are separated into rocks attributed to ridge versus post-ridge magmatism. Published data are from *McCulloch et al*. [1981], *Godard et al*. [2006], *Amri et al*. [2007], and *Rioux et al*. [2012a]. All of the Nd data discussed herein are re-calculated to be consistent with the fractionation correction used in this study. The abbreviations used are defined as: plut.—plutonic; ton./trond.—tonalite/trondhjemite.

three tonalites have imprecise older dates, but the older dates are within uncertainty of more precise, younger dates from nearby gabbros. The data are again discussed in the context of the different ophiolite massifs.

5.3.1. Wadi Tayin Massif

[29] To better constrain the timing of movement along the metamorphic sole of the ophiolite, we dated a trondhjemitic pod from the metamorphic sole in the Wadi Tayin massif (CWO14; collected and originally dated by *Warren et al*., [2005]) and analyzed the Nd isotopic composition of a second trondhjemite pod from the same exposure (9131M08). *Warren et al*. [2005] interpreted the trondhjemite pods to be leucocratic melts of the sole [*Warren et al*., 2005], though they could also be intrusions of partial melts from a deeper source. The first trondhjemite yielded a cluster of younger dates between 94.90 ± 0.38 and 94.69 ± 0.12 Ma and a single older date of 170.29 ± 0.24 Ma, which we interpret as an inherited xenocryst. The second trondhjemite had an $\varepsilon_{Nd}(96\ Ma) = -7.01$ 0.16, indicating it was derived from a source with a time-integrated enrichment in LREE.

5.3.2. Samail Massif

[30] As discussed above, field relations suggest that the northeast and southwest sections of the Samail massif are remnants of older crust that was intruded by a younger NW-SE oriented ridge. The two on-axis gabbros from the center of the massif yielded $^{206}Pb/^{238}U$ dates of 96.441 ± 0.062 to 95.69 ± 0.17 Ma. In addition to these gabbros, we dated two tonalites from the middle and lower crust in the center of the massif: a tonalite stock that intrudes the layered gabbro/upper level gabbro boundary (OM01-05) and a meter-scale tonalite sill that intrudes layered gabbro directly above the crust-mantle transition (9127M01) (Figure 1d). $^{206}Pb/^{238}U$ dates from the two samples overlap within uncertainty and range from 95.706 ± 0.062 to 95.402 ± 0.054 Ma, younger than both of the nearby on-axis gabbros (Figure 4). 9127M01 had $\varepsilon_{Nd}(96\ Ma) = 6.90 \pm 0.12$ (Figure 3).

[31] In addition, we dated three samples from the northeastern section of the massif, which field evidence suggests is older than the central part of the massif. The dated samples include an upper level gabbro (9124M05), a tonalite dike that intrudes upper level gabbro and is mingled with a mafic dike (9124M07; "vinaigrette" texture) and a tonalite that intrudes the upper level gabbro-sheeted dike contact (CWO18) (Figure 1d). The gabbro sample has $^{206}Pb/^{238}U$ dates of 95.5 ± 0.17 to 95.285 ± 0.082 Ma. The $^{206}Pb/^{238}U$ dates from the two trondhjemite samples have larger uncertainties, but the most precise dates range from 95.76 ± 0.25 to 95.36 ± 0.27 Ma, consistent with the gabbro dates. Initial Nd isotopic ratios from two of the dated samples have $\varepsilon_{Nd}(96\ Ma) = 7.19 \pm 0.12$ and 7.25 ± 0.16 (9124M05, 9124M07) (Figure 3). The dates are ~0.5 Ma younger than the dates from the older, on-axis gabbros in the center of the massif. Given the structural evidence that the crustal section in the northeast of the massif is older that the center of the massif, we attribute the three younger rocks from the northeast section to younger magmatism that post-dates formation of the on-axis crust. This magmatism may be associated with the nearby Mansah diapir, which has been interpreted as an off-axis diapir that intruded cooling lithosphere [*Jousselin and Nicolas*, 2000]. Low-Cr# chromium spinels from basaltic dikes in the mantle in this area have

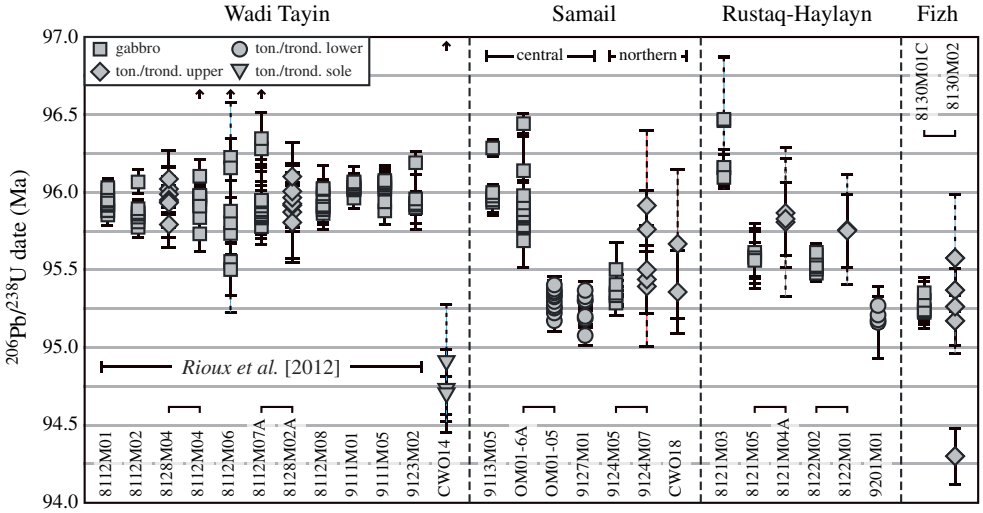

Figure 4. ^{206}Pb/^{238}U dates from plutonic samples within the ophiolite organized by massif. Data are from this study and *Rioux et al*. [2012a]. Closely spaced pairs of gabbroic and felsic plutonic samples are linked with brackets. Older grains from samples 8112M04, 8112M06, 8112M07A, and CWO14 plot off-scale (denoted with arrows). Samples 8111M02 and 9114M01A from *Rioux et al*. [2012a] were excluded (see discussion in section 3). Analyses with 2σ uncertainties ≥0.5 Ma are excluded for clarity, and analyses with 2σ uncertainties ≥0.3 Ma are plotted with dashed error bars.

also been attributed to either variations in the degree of mantle melting or off-axis magmatism [*Python et al*., 2008].

5.3.3. Haylayn Massif

[32] In the Haylayn massif, numerous small granite, granodiorite, tonalite, and trondhjemite sills and dikes intrude into mantle harzburgite below the crust-mantle transition. Isotopic and geochemical data from these intrusions have low ε_{Nd}(96 Ma) = −5.6 to −5.8 and high initial ^{87}Sr/^{86}Sr = 0.7086–0.7094 [97RU7, 97RU8; *Amri et al*., 2007] and are enriched in LREE and fluid mobile trace elements [*Amri et al*., 2007; *Rollinson*, 2009]. The structural position of the intrusions is similar to granitoids with low ε_{Nd}(t) that intrude into mantle harzburgites in the northern ophiolite massifs [*Briqueu et al*., 1991; *Cox et al*., 1999]. The range of Nd isotopic compositions for post-ridge dikes and sills in the mantle from throughout the ophiolite are shown in Figure 3.

[33] To determine how these intrusions relate to ridge magmatism and/or emplacement of the ophiolite, we analyzed a trondhjemite dike in harzburgite directly below the crust-mantle transition in the Haylayn massif (9201M01). The dike yielded ^{206}Pb/^{238}U dates of 95.270 ± 0.056 to 95.177 ± 0.051 Ma (excluding a single lower precision analysis that overlaps within uncertainty) and had low ε_{Nd} (96 Ma) = −7.77 ± 0.08.

[34] An additional sample from a cluster of granitic dikes that intrude harzburgite far from the crust-mantle transition in the Haylayn massif (OM01-70) (Figure 1c) yielded a strikingly young ^{206}Pb/^{238}U date of 77.22 ± 0.65 Ma and a

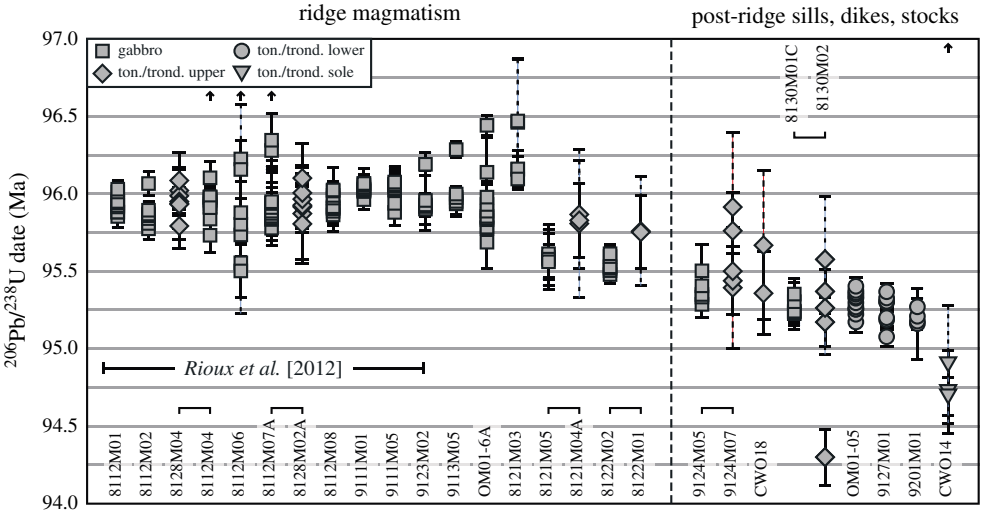

Figure 5. ^{206}Pb/^{238}U dates from plutonic samples within the ophiolite organized following the interpretations discussed in the text. Data are from this study and *Rioux et al*. [2012a]. See Figure 4 caption for a full description of the included/excluded data.

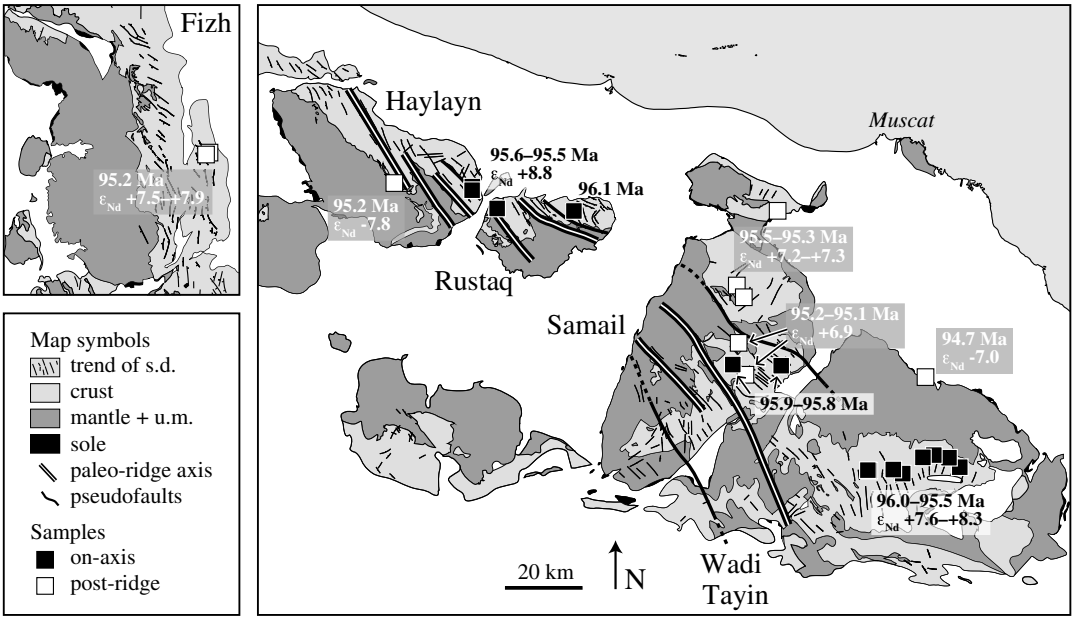

Figure 6. Summary and interpretation of the $^{206}Pb/^{238}U$ dates and Nd isotopic data. Map, paleo-ridge, and pseudofault locations are modified from *Nicolas et al*. [2000]. Ranges of dates (Ma) are interpreted final crystallization ages based on the youngest precise date from each sample/location and exclude older xenocrysts. Black sample locations are from on-axis samples, and white sample locations are from post-ridge dikes, sills, and stocks. Pseudofaults [*Hey*, 1977] mark the boundaries between younger propagating crust and older oceanic lithosphere.

group of older dates that range from 95.24 ± 0.43 to 93.74 ± 0.18 Ma. The younger date is similar to the age of peak metamorphism during subduction of the Arabian continent (~79 Ma) [*Warren et al*., 2005], and this dike may be related to final obduction of the ophiolite onto the continental margin.

5.3.4. Fizh Massif

[35] The Fizh area has a complex magmatic history. In the study area, the volcanic record includes thick sections of both the MORB-like V1 (Geotimes) unit and overlying V2 lavas (Figure 1b) [*Alabaster et al*., 1982; *Godard et al*., 2003]. Multiple generations of plutonism have also been identified in the Fizh massif [*Adachi and Miyashita*, 2003; *MacLeod and Rothery*, 1992; *Reuber*, 1988], and some of the plutonic rock have been chemically correlated with the extrusive volcanic units [*Adachi and Miyashita*, 2003].

[36] We dated two samples from the eastern part of the massif: an upper level gabbro (8130M01C) and nearby tonalite dike (8130M02) (Figure 1b). The gabbro yielded $^{206}Pb/^{238}U$ dates of 95.35 ± 0.10 to 95.23 ± 0.10 Ma and the most precise $^{206}Pb/^{238}U$ dates from the trondhjemite range from 95.37 ± 0.14 to 95.17 ± 0.18 Ma, excluding a younger analysis (94.30 ± 0.18 Ma) that we interpret to be affected by residual Pb loss. The two samples have $\varepsilon_{Nd}(96\ Ma) = 7.88 \pm 0.16$ and 7.48 ± 0.16, respectively. The dates are younger than the on-axis samples from this study and *Rioux et al*. [2012a] from the Wadi Tayin, Samail, Rustaq, and Haylayn massifs (Figures 1, 4, and 5) and most of the published $^{206}Pb/^{238}U$ dates from two pegmatitic gabbros and a felsic body that intrude the main portion of ophiolite crust in the UAE [*Goodenough et al*., 2010]; uncorrected $^{206}Pb/^{238}U$ dates from the Goodenough study range from 95.76 ± 0.48 to 95.22 ± 0.37 Ma, while the uncorrected dates from 8130M01C range from 95.271 ± 0.099 to 95.15 ± 0.10 Ma. Given that the Fizh samples are younger than the on-axis magmatism from this study and *Rioux et al*. [2012a], and most of the dates of secondary magmatism in the UAE from *Goodenough et al.* [2010], we interpret the two dated samples from the Fizh massif to be late, off-axis intrusions into older on-axis crust, likely related to the locally voluminous V2 volcanism.

5.3.5. Summary

[37] All of the $^{206}Pb/^{238}U$ dates of the younger group of samples, with the exception of the trondhjemites from the metamorphic sole, overlap within uncertainty, indicating that late gabbroic, tonalitic, and trondhjemitic magmas intruded all levels of the ophiolite 0.25–0.75 Ma after formation of the ophiolite crust. While all of the magmas were intruded over a short time interval, they tapped at least two isotopically distinct sources. The late gabbro and tonalite from the Samail massif (9124M05, 9124M07, 9127M01) and Fizh massif (9130M01C, 9130M02) have $\varepsilon_{Nd}(96\ Ma) = 6.90$ to 7.88. In contrast, the trondhjemitic dike that intrudes harzburgite in the Haylayn massif (9201M01) has $\varepsilon_{Nd}(96\ Ma) = -7.77$. The trondhjemitic pod from the metamorphic sole (9131M08) is 0.5–1.25 Ma younger than the ridge-related magmas and a similar nearby pod has $\varepsilon_{Nd}(96\ Ma) = -7.01$.

5.4. Source of Post-Ridge Dikes, Sills, and Stocks With Positive $\varepsilon_{Nd}(t)$

[38] The Nd isotopic data from the post-ridge sills, dikes, and stocks that intrude the crust overlap, but extend to lower values, than Nd isotopic data from crustal rocks attributed to ridge magmatism (Figure 3c). Existing data from ridge-related rocks, including gabbros, tonalites,

trondhjemites, sheeted dikes, and V1 lavas have ε_{Nd} (96 Ma) > 7.5. The late sills, dikes, and stocks from the crust analyzed in this study have $\varepsilon_{Nd}(96\ Ma) = 6.90 \pm 0.12$ to 7.88 ± 0.16. Similarly, V2 volcanic rocks analyzed by *Godard et al*. [2006] extend to slightly lower values than the ridge-related samples, with four samples ranging from $\varepsilon_{Nd}(96\ Ma) = 7.26 \pm 0.23$ to 8.68 ± 0.14. The overlap in isotopic composition between the ridge-related rocks and the highest $\varepsilon_{Nd}(t)$ samples from the post-ridge intrusive and volcanic rocks suggests that both the ridge and secondary magmas in the crust were derived from a similar mantle source. However, the extension to lower $\varepsilon_{Nd}(t)$ for the secondary magmas suggests that a low $\varepsilon_{Nd}(t)$ component was added to the mantle source, likely reflecting a progressive increase in fluids and/or melts derived from a subducting slab or underthrust plate.

[39] Interestingly, Nd isotopic data from *Benoit et al*. [1996] from troctolite to gabbronorite intrusions into mantle harzburgites surrounding the Maqsad mantle diapir have a significantly larger range in isotopic values ($\varepsilon_{Nd}(96\ Ma) = 6.08 \pm 0.18$ to 10.22 ± 0.31) than either the ridge-related or secondary magmas in the crust (Figure 3b). A focused study of the isotopic composition of crustal rocks structurally above the diapir is needed to test whether the crustal rocks in this area display a similar range of isotopic heterogeneity or if the heterogeneity is restricted to the mantle.

5.5. Source of Post-Ridge Dikes, Sills and Stocks With Negative $\varepsilon_{Nd}(t)$

[40] The negative $\varepsilon_{Nd}(t)$ values observed in this and earlier studies clearly indicate that some of the post-ridge dikes and sills that intrude the mantle must be related to dehydration, melting, and/or assimilation of material with time-integrated LREE enrichment. Potential sources for the negative $\varepsilon_{Nd}(t)$ signature could include continental crust, terrigenous sediments, or hydrothermal or hydrogenous sediments, which scavenge "continental" Nd from sea water [*Chavagnac et al*., 2006; *German et al*., 1990; *Goldstein and O'Nions*, 1981; *Halliday et al*., 1992; *Olivarez and Owen*, 1989].

[41] If the ophiolite was thrust over similar crust near the ridge axis, the sediments that are preserved within the V1 volcanic series and between the V1 and V2 volcanic series could provide insight into the sedimentary package in the downgoing plate. The preserved sediments consist of thin lenses of siliceous metalliferous sediments, interpreted to reflect siliceous oozes and hydrothermal deposits [*Ernewein et al*., 1988; *Fleet and Robertson*, 1980; *Karpoff et al*., 1988; *Robertson and Fleet*, 1986]. Similar sediments from modern ridges often have negative $\varepsilon_{Nd}(t)$ [*Chavagnac et al*., 2006; *Goldstein and O'Nions*, 1981; *Halliday et al*., 1992], and these could be a potential source for the negative $\varepsilon_{Nd}(t)$ of the dikes and sills that intrude the mantle. However, limited geochemical analyses from the Oman sediments are characterized by flat REE patterns with large negative Ce anomalies [*Robertson and Fleet*, 1986], which are typical of hydrothermal metalliferous sediments from the modern oceans [*Barrett and Jarvis*, 1988; *German et al*., 1990; *Hole et al*., 1984]. In contrast, the dikes and sills in the mantle have steep LREE patterns with little or no Ce anomaly [*Amri et al*., 2007; *Rollinson*, 2009], suggesting the REE (including Nd) were not derived from similar sediments. It is also unlikely that the low Nd isotopic ratios of the sills and dikes can be explained by melting of hydrothermally altered crust or mantle because sea water, unlike hydrothermal metalliferous sediments, contains very low concentrations of Nd [*Elderfield and Greaves*, 1982] and hydrothermal alteration does not result in large shifts in Nd isotopic compositions [*Hart et al*., 1999; *Valsami-Jones and Cann*, 1994].

[42] Instead, we favor the interpretation that the low $\varepsilon_{Nd}(t)$ of the late dikes is related to melting, dehydration, or assimilation of continentally derived sediments or crust in the underthrust/subducted plate. Previous studies of dikes, sills, and stocks with negative $\varepsilon_{Nd}(t)$ in the mantle section in the UAE concluded that the intrusions are best explained by partial melting of terrigenous quartzofeldspathic sediments and a basaltic component in the metamorphic sole and Haybi complex [*Briqueu et al*., 1991; *Cox et al*., 1999]. These conclusions are supported by isotopic analyses which show that the underthrust metasediments have $\varepsilon_{Nd}(96\ Ma) = -6$ to -14. There are fewer isotopic analyses of rocks exposed in the sole exposures in the Oman part of the ophiolite; however, the trondhjemitic pod that we analyzed in this study from the Wadi Tayin sole exposure also had a strongly negative $\varepsilon_{Nd}(96\ Ma) = -7.0$, suggesting that anatectic melting of the sole is also a viable source for the negative $\varepsilon_{Nd}(t)$ in the ophiolite massifs in Oman.

[43] An important corollary to this interpretation is that it implies that the underthrust/subducted plate had a different composition than the ophiolite crust and overlying sediments. This interpretation was proposed by *Searle and Malpas* [1982] and is supported by the isotopic data discussed above, the different thickness and composition of sediments in the underthrust sheet versus within the ophiolite volcanic sequences, and the differences in the trace element composition of the ophiolite crust and mafic rocks in the metamorphic sole [*Searle and Cox*, 2002; *Searle and Malpas*, 1982; *Warren et al*., 2007]. The compositional differences between the underthrust and overriding plates could be a result of the ophiolite being thrust over adjacent continental crust, trench fill sediments or older oceanic crust with a thicker and compositionally distinct sedimentary package, as a result of either thrusting across a transform plate boundary or subduction below the ophiolite.

[44] The new U-Pb zircon dates from the mantle dike in the Haylayn massif ($\varepsilon_{Nd}(96\ Ma) = -7.77$) indicate that the crustal material or terrigenous sediments were thrust or subducted below the ophiolite ≤0.25–0.5 Ma after formation of the ophiolite crust (Figure 5). The small offset between crustal growth by on-axis ridge magmatism and the development of subduction or thrusting below the ophiolite is consistent with the existing $^{40}Ar/^{39}Ar$ thermochronology, which documented similar cooling dates for plutonic rocks in the crust and metamorphic rocks in the sole of the ophiolite, suggesting rapid development and cooling of the metamorphic sole following ridge magmatism [*Hacker*, 1994; *Hacker et al*., 1996].

5.6. Temporal Constraints on the Tectonic Development of the Ophiolite

[45] The new U-Pb zircon dates and whole rock Sm-Nd data place temporal constraints on models for the formation and emplacement of the ophiolite. Current tectonic models can be broadly grouped into two categories: (1) formation

at a typical mid-ocean ridge spreading center, followed by emplacement along a shallow thrust (Figure 7b) [*Boudier and Coleman*, 1981; *Boudier and Nicolas*, 2007; *Boudier et al*., 1988; *Gregory et al*., 1998; *Hacker*, 1991; *Hacker et al*., 1996; *Nicolas and Boudier*, 2003], and (2) formation and emplacement in a supra-subduction zone setting [*Alabaster et al*., 1982; *Pearce et al*., 1981; *Searle and Cox*, 2002; *Searle and Malpas*, 1980; *Warren et al*., 2005]. In supra-subduction zone models, the geochemical progression of the Oman lavas, including the presence of boninitic lavas in the V2 series and similarities between ophiolites and fore-arc crust in western Pacific arcs, have led many authors to propose that the Samail and other ophiolites may have formed during subduction initiation (Figure 7C) [*Bloomer et al*., 1995; *Casey and Dewey*, 1984; *Dilek and Flower*, 2003; *Flower and Dilek*, 2003; *Reagan et al*., 2010; *Stern*, 2004; *Stern and Bloomer*, 1992].

[46] The data presented here and in *Rioux et al*. [2012a] indicate that (1) Gabbros, tonalites, and trondhjemites attributed to on-axis ridge magmatism crystallized between ~96.25 and 95.50 Ma; (2) formation of the ophiolite crust was followed by intrusion of two coeval magmatic series in the crust and mantle between ~95.4 and 95.0 Ma; rocks in the crust have ε_{Nd}(t) similar to, but slightly lower than, on-axis gabbros, whereas the dated dike in the mantle has a negative ε_{Nd}(t). The negative ε_{Nd}(t) of the dike in the mantle requires that subduction or thrusting below the ophiolite was established ≤0.25–0.5 Ma after formation of the crust; and (3) U-Pb dates from the trondhjemite pod in the metamorphic sole are slightly younger and record dates of ~94.7 Ma, suggesting the sole was still hot and/or wet enough to melt at this time.

[47] The U-Pb dates and isotopic data do not definitively differentiate between mid-ocean ridge and supra-subduction zone models, and the data can be interpreted differently in each case. In mid-ocean ridge models, where thrusting/subduction develop after formation of the ophiolite crust, the post-ridge sills and dikes in the mantle and trondhjemites in the metamorphic sole with negative $\varepsilon_{Nd}(t)$ can be interpreted to reflect melting and/or assimilation of material from the underthrust plate during initial development of the emplacement thrust. In this case, initial thrusting occurred 0.25–0.5 Ma after formation of the crust and the sole stayed hot enough to partially melt for ~0.5 Ma. The small age difference between ridge magmatism and magmatism related to initial thrusting is consistent with the thrust forming close to the ridge axis, allowing thrust-related magmas to rapidly intrude into recently formed crust. The U-Pb dates indicate that late gabbroic dikes and sills in the crust, which we tentatively correlate with the V2 volcanic series, are coeval with this initial thrusting.

[48] Two aspects of the post-ridge magmatism are difficult to understand in mid-ocean ridge models: (1) The boninitic composition of some lavas suggests that parental magmas formed at >1200°C [*Ishikawa et al*., 2002], but it is unlikely that the mantle wedge above the emplacement thrust remained at such high temperatures [*Hacker*, 1990]. (2) The negative $\varepsilon_{Nd}(t)$ of the mantle dikes suggests that the underthrust plate had a distinct composition from the preserved ophiolite crust and overlying sediments. The latter could be explained by thrusting across an oceanic transform with initial thrusting parallel to the ridge axis and the preserved length of the ophiolite.

[49] In a supra-subduction zone setting, the U-Pb dates and Nd isotopic data may reflect the evolution/development of subduction. In this case, the on-axis magmatism that formed most of the crust would likely be related to slab roll back, potentially reflecting initial subsidence of a plate during subduction initiation [e.g., *Hall et al*., 2003; *Stern*, 2004; *Stern and Bloomer*, 1992]. Spreading may have occurred at multiple small spreading centers within the extending upper plate, consistent with the evidence for ridge propagation within the ophiolite. The intrusion of the two younger magmatic series would likely be related to maturation of the subducting slab to conditions conducive to melting and/or fluid release. The bimodal isotopic composition of the late sills, dikes, and stocks are consistent with coeval decompression and/or fluid-fluxed melting of the mantle wedge (positive ε_{Nd}) and melting, dehydration, or assimilation of sediment in the down going slab (negative ε_{Nd}). Thermal models of subduction initiation suggest that geotherms above the slab are steeper than in mature subduction zones [*Hall et al*., 2003], which could facilitate sediment melting. In subduction initiation models, the V2 volcanism has been attributed to initial development of a proto-arc. If this interpretation is correct, and the young sills, dikes, and stocks from the crust that we dated are the intrusive equivalent of the V2 lavas, the difference between the older on-axis gabbros and younger magmatic series implies that it can take <0.25–0.75 Ma to evolve from spreading related to slab role back to proto-arc volcanism in a young subduction zone. The younger dates from the ophiolite sole may reflect a change in subduction parameters, which led to shallowing of the thrust, initial emplacement of the ophiolite, and the termination of proto-arc volcanism.

[50] We currently favor the later model (Figure 7c), which better explains the origin of the younger magmatic series. This interpretation is supported by a recent compilation of major element data, which shows compelling evidence for the presence of hydrous magmas in both the on-axis and off-axis suites [*MacLeod et al*., 2013].

6. Conclusion

[51] We report new high-precision single grain and grain fragment U/Pb zircon dates from 17 gabbros, tonalites, and trondhjemites from the Wadi Tayin, Samail, Rustaq, Haylayn, and Fizh massifs and Nd isotopic data from eight of the sample locations. The dated samples can be divided into two groups: an older group of gabbros, tonalites, and trondhjemites attributed to ridge magmatism during crustal accretion; and a younger group of post-ridge dikes, sills, and stocks that intrude all levels of the ophiolite. The former gabbros, tonalites, and trondhjemites yielded $^{206}Pb/^{238}U$ dates of 96.441 ± 0.062 to 95.478 ± 0.056 Ma and a single gabbro from the Rustaq massif has $\varepsilon_{Nd}(96\ Ma) = 8.83 \pm 0.20$. These results are consistent with our recent work in the Wadi Tayin massif, where 12 on-axis gabbros, tonalites, and trondhjemites had $^{206}Pb/^{238}U$ dates of 99.15 ± 0.10 to 95.50 ± 0.17 Ma, with most data clustered between 96.40 ± 0.17 and 95.50 ± 0.17 Ma, and seven of the dated samples and one undated sample had $\varepsilon_{Nd}(96\ Ma) = 7.59 \pm 0.23$ to 8.28 ± 0.31 [*Rioux et al*., 2012a]. The

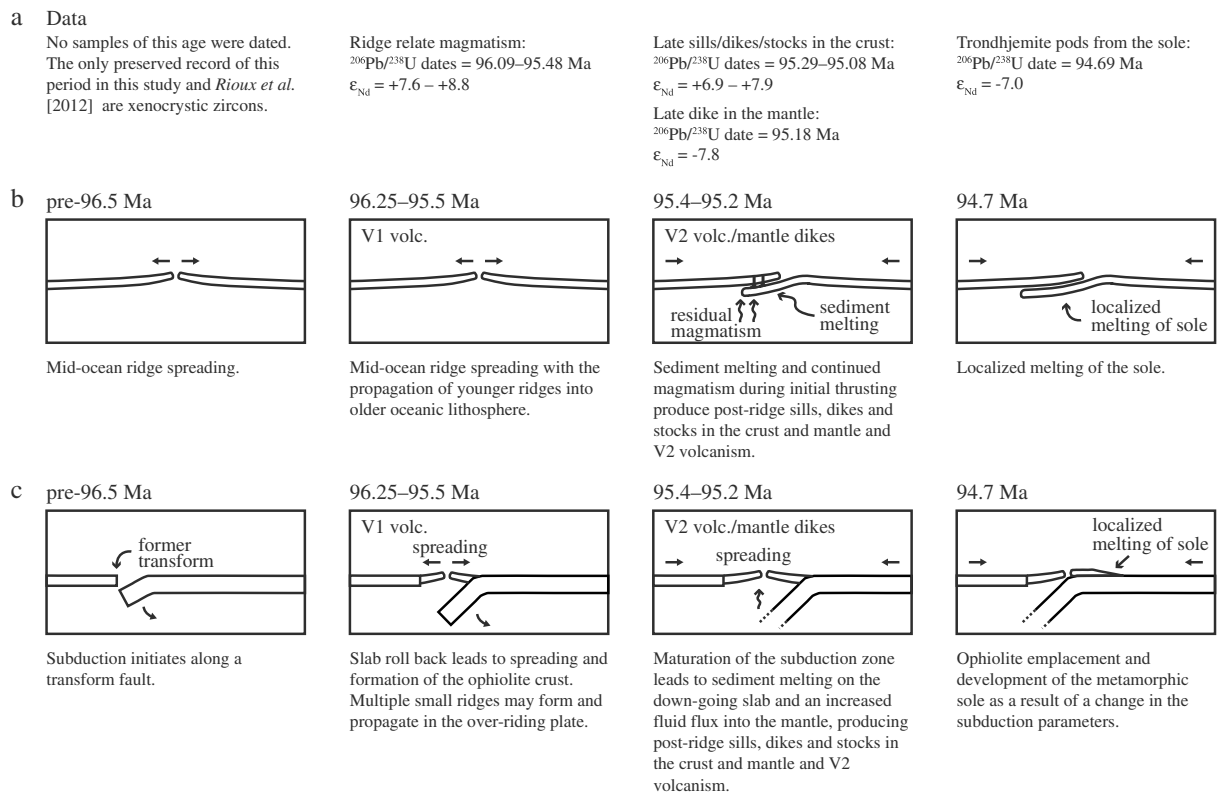

Figure 7. Tectonic models for ophiolite formation. (a) Data from this study and *Rioux et al*. [2012a] that constrain the tectonic development of the ophiolite. The reported range in $^{206}Pb/^{238}U$ dates was determined using the youngest precise date for each sample. (b) Formation at a mid-ocean ridge followed by thrusting along the ridge axis [e.g., *Boudier et al*., 1988]. (c) Formation by subduction initiation [e.g., *Bloomer et al*., 1995; *Stern and Bloomer*, 1992].

combined datasets suggest that most of the ophiolite crusts formed by on-axis ridge magmatism in <1 Ma and are consistent with structural evidence for ridge propagation during crustal growth. The Nd isotopic data are similar to modern MORB, indicating that the crust-forming magmas were derived from a MOR type mantle source.

[52] The younger dikes, sills, and stocks from the crust and mantle have $^{206}Pb/^{238}U$ dates of 95.077 ± 0.062 to 95.405 ± 0.062 Ma. A trondhjemite pod in the metamorphic sole has younger $^{206}Pb/^{238}U$ dates of 94.90 ± 0.38 to 94.69 ± 0.12 Ma. Nd isotopic data from these samples are bimodal: tonalites and gabbros from all levels of the crust have $\varepsilon_{Nd}(96\ Ma) = 6.90 \pm 0.12$ to 7.88 ± 0.16, while a trondhjemite dike that intrudes mantle harzburgite and a trondhjemite pod in the sole have $\varepsilon_{Nd}(96\ Ma) = -7.77 \pm 0.08$ and -7.01 ± 0.16, respectively. The combined data suggest that while the magmatism in the crust and mantle were coeval, they were generated from at least two isotopically distinct sources. The data from the trondhjemite dike in the mantle with negative $\varepsilon_{Nd}(t)$ require that material with time-integrated LREE enrichment was thrust below the ophiolite ≤0.25–0.5 Ma after formation of the ophiolite crust. The Nd isotopic composition of the post-ridge intrusions in the crust, which are most likely related to the V2 volcanic series, are similar to, but slightly lower than, on-axis rocks, consistent with progressive addition of an enriched fluid or melt to the mantle source. The bimodal isotopic compositions of the late dikes, sills, and stocks can be explained by coeval decompression and/or fluid-fluxed melting of the mantle and melting, dehydration, or assimilation of sediment in the underthrust plate during the development of thrusting or subduction.

[53] **Acknowledgments.** We thank Adolphe Nicolas and Françoise Boudier for their insight in the field in Oman and many discussions of the geology of the ophiolite and the data presented here. We also thank Brad Hacker for discussions on the formation and emplacement of the ophiolite, Clare Warren for sharing zircon separates from two of her samples, and Georges Ceuleneer and Mathieu Benoit for sharing and discussing their geochemical data. We thank Jessica Creveling and Linnea Koons for separating zircons from many of the dated samples. We are grateful to the Ministry of Commerce and Industry, Directorate General of Minerals in Oman for helping to facilitate our fieldwork within the ophiolite. The manuscript was significantly improved by detailed and constructive reviews by Adolphe Nicolas, Marguerite Godard, and Delphine Bosch. This research was funded by NSF grant OCE-0727914.

References

Adachi, Y., and S. Miyashita (2003), Geology and petrology of the plutonic complexes in the Wadi Fizh area: Multiple magmatic events and segment structure in the northern Oman ophiolite, *Geochem. Geophys. Geosyst.*, *4*(9), 8619.

Alabaster, T., J. A. Pearce, and J. Malpas (1982), The volcanic stratigraphy and petrogenesis of the Oman ophiolite complex, *Contrib. Mineral. Petrol.*, *81*(3), 168–183.

Amri, I., M. Benoit, and G. Ceuleneer (1996), Tectonic setting for the genesis of oceanic plagiogranites: Evidence from a paleo-spreading structure in the Oman ophiolite, *Earth Planet. Sci. Lett.*, *139*(1–2), 177–194.

Amri, I., G. Ceuleneer, M. Benoit, M. Python, E. Puga, and K. Targuisti (2007), Genesis of granitoids by interaction between mantle peridotites and hydrothermal fluids in oceanic spreading setting in the Oman ophiolite, *Geogaceta*, *42*, 23–26.

Barrett, T. J., and I. Jarvis (1988), Rare-earth element geochemistry of metalliferous sediments from DSDP Leg 92: The East Pacific Rise transect, *Chem. Geol.*, *67*(3–4), 243–259.

Benoit, M., M. Polvé, and G. Ceuleneer (1996), Trace element and isotopic characterization of mafic cumulates in a fossil mantle diapir (Oman ophiolite), *Chem. Geol.*, *134*(1–3), 199–214.

Beurrier, M., F. Béchennec, G. Hutin, and D. Rabu (1986a), As Suwayq-Sheet NF40-3A Geologic Map, Ministry of Petroleum and Minerals, Directorate General of Minerals, Sultanate of Oman.

Beurrier, M., F. Béchennec, G. Hutin, and D. Rabu (1986b), Rustaq-Sheet NF40-3D Geologic Map, Ministry of Petroleum and Minerals, Directorate General of Minerals, Sultanate of Oman.

Bibby, L. E. (2013), "Moist MORB" axial magmatism in the Oman ophiolite: The evidence against a mid-ocean ridge origin, *Geology*, doi:10.1130/G33904.1.

Bishimetal Exploration Co. Ltd. (1987), Wadi Bani Umar-Sheet NF40-14E-II Geologic Map, Ministry of Petroleum and Minerals, Directorate General of Minerals, Sultanate of Oman.

Bloomer, S. H., B. Taylor, C. J. MacLeod, R. J. Stern, P. Fryer, J. W. Hawkins, and L. Johnson (1995), Early arc volcanism and the ophiolite problem: A perspective from drilling in the western Pacific, in *Active Margins and Marginal Basins of the Western Pacific*, edited, pp. 1–30, AGU, Washington, DC.

Boudier, F., and R. G. Coleman (1981), Cross section through the peridotite in the Samail ophiolite, southeastern Oman Mountains, *J. Geophys. Res.*, *86*(B4), 2573–2592.

Boudier, F., and A. Nicolas (2007), Comment on "dating the geologic history of Oman's Semail ophiolite: Insights from U–Pb geochronology" by C. J. Warren, R. R. Parrish, D. J. Waters and M. P. Searle, *Contrib. Mineral. Petrol.*, *154*(1), 111–113.

Boudier, F., G. Ceuleneer, and A. Nicolas (1988), Shear zones, thrusts and related magmatism in the Oman ophiolite: Initiation of thrusting on an oceanic ridge, *Tectonophysics*, *151*(1–4), 275–296.

Boudier, F., M. Godard, and C. Armbruster (2000), Significance of gabbronorite occurrence in the crustal section of the Semail ophiolite, *Mar. Geophys. Res.*, *21*(3), 307–326.

Boudier, F., A. Nicolas, B. Ildefonse, and D. Jousselin (1997), EPR microplates, a model for the Oman Ophiolite, *Terra Nova*, *9*(2), 79–82.

Bowring, J. F., N. M. McLean, and S. A. Bowring (2011), Engineering Cyber Infrastructure for U-Pb Geochronology: Tripoli and U-Pb_Redux, *Geochem. Geophys. Geosyst.*, doi:10.1029/2010GC003479.

Briqueu, L., C. Mével, and F. Boudier (1991), Sr, Nd and Pb isotopic constraints on the genesis of a calc-alkaline plutonic suite in the Oman mountains related to the obduction process, in *Ophiolite Genesis and Evolution of the Oceanic Lithosphere*, edited by P. Tea, pp. 517–542, Ministry of Petroleum and Minerals, Sultanate of Oman.

Browning, P. (1984), Cryptic variation within the Cumulate Sequence of the Oman ophiolite: Magma chamber depth and petrological implications, *Geol. Soc. London, Spec. Pub.*, *13*(1), 71–82.

Casey, J. F., and J. F. Dewey (1984), Initiation of subduction zones along transform and accreting plate boundaries, triple-junction evolution, and forearc spreading centres—Implications for ophiolitic geology and obduction, *Geol. Soc. London, Spec. Pub.*, *13*(1), 269–290.

Chavagnac, V., M. R. Palmer, J. A. Milton, D. R. H. Green, and C. R. German (2006), Hydrothermal sediments as a potential record of seawater Nd isotope compositions: The Rainbow vent site (36°14′N, Mid-Atlantic Ridge), *Paleoceanography*, *21*(3), PA3012, doi:10.1029/2006PA001273.

Chévremont, P., J. Le Métour, R. Wyns, F. Béchennec, D. Janjou, and J. Roger (1993), Fizh-Sheet NF40-14B4 Geologic Map, Ministry of Petroleum and Minerals, Directorate General of Minerals, Sultanate of Oman.

Coogan, L. A., G. Thompson, and C. J. MacLeod (2002a), A textural and geochemical investigation of high level gabbros from the Oman ophiolite: Implications for the role of the axial magma chamber at fast-spreading ridges, *Lithos*, *63*(1–2), 67–82.

Coogan, L. A., G. R. T. Jenkin, and R. N. Wilson (2002b), Constraining the cooling rate of the lower oceanic crust: A new approach applied to the Oman ophiolite, *Earth Planet. Sci. Lett.*, *199*(1–2), 127–146.

Cox, J., M. Searle, and R. Pedersen (1999), The petrogenesis of leucogranitic dykes intruding the northern Semail ophiolite, United Arab Emirates: Field relationships, geochemistry and Sr/Nd isotope systematics, *Contrib. Mineral. Petrol.*, *137*(3), 267–287.

Dilek, Y., and M. F. J. Flower (2003), Arc-trench rollback and forearc accretion: 2. A model template for ophiolites in Albania, Cyprus, and Oman, *Geol. Soc. London, Spec. Publ.*, *218*(1), 43–68.

Elderfield, H., and M. J. Greaves (1982), The rare earth elements in seawater, *Nature*, *296*(5854), 214–219.

Ernewein, M., C. Pflumio, and H. Whitechurch (1988), The death of an accretion zone as evidenced by the magmatic history of the Sumail ophiolite (Oman), *Tectonophysics*, *151*(1–4), 247–274.

Fleet, A. J., and A. H. F. Robertson (1980), Ocean-ridge metalliferous and pelagic sediments of the Semail Nappe, Oman, *J. Geol. Soc.*, *137*(4), 403–422.

Flower, M. F. J., and Y. Dilek (2003), Arc-trench rollback and forearc accretion: 1. A collision-induced mantle flow model for Tethyan ophiolites, *Geol. Soc. London, Spec. Publ.*, *218*(1), 21–41.

France, L., B. Ildefonse, and J. Koepke (2009), Interactions between magma and hydrothermal system in Oman ophiolite and in IODP Hole 1256D: Fossilization of a dynamic melt lens at fast spreading ridges, *Geochem. Geophys. Geosyst.*, *10*(10), Q10O19, doi:10.1029/2009GC002652.

German, C. R., G. P. Klinkhammer, J. M. Edmond, A. Mura, and H. Elderfield (1990), Hydrothermal scavenging of rare-earth elements in the ocean, *Nature*, *345*(6275), 516–518.

Gnos, E. (1998), Peak metamorphic conditions of garnet amphibolites beneath the Semail Ophiolite: Implications for an inverted pressure gradient, *Int. Geol. Rev.*, *40*(4), 281–304.

Gnos, E., and T. Peters (1993), K-Ar ages of the metamorphic sole of the Semail Ophiolite: Implications for ophiolite cooling history, *Contrib. Mineral. Petrol.*, *113*(3), 325–332.

Gnos, E., and D. Kurz (1994), Sapphirine-quartz and sapphirine-corundum assemblages in metamorphic rocks associated with the Semail Ophiolite (United Arab Emirates), *Contrib. Mineral. Petrol.*, *116*(4), 398–410.

Godard, M., J. M. Dautria, and M. Perrin (2003), Geochemical variability of the Oman ophiolite lavas: Relationship with spatial distribution and paleomagnetic directions, *Geochem. Geophys. Geosyst.*, *4*(6), 8609.

Godard, M., D. Bosch, and F. Einaudi (2006), A MORB source for low-Ti magmatism in the Semail ophiolite, *Chem. Geol.*, *234*(1–2), 58–78.

Goldstein, S. L., and R. K. O'Nions (1981), Nd and Sr isotopic relationships in pelagic clays and ferromanganese deposits, *Nature*, *292*(5821), 324–327.

Goodenough, K., M. Styles, D. Schofield, R. Thomas, Q. Crowley, R. Lilly, J. McKervey, D. Stephenson, and J. Carney (2010), Architecture of the Oman–UAE ophiolite: Evidence for a multi-phase magmatic history, *Arabian J. Geosci.*, *3*(4), 439–458.

Gregory, R. T., D. R. Gray, and J. Miller (1998), Tectonics of the Arabian margin associated with the formation and exhumation of high-pressure rocks, Sultanate of Oman, *Tectonics*, *17*(5), 657–670.

Hacker, B. R. (1990), Simulation of the metamorphic and deformational history of the metamorphic sole of the Oman ophiolite, *J. Geophys. Res.*, *95*(B4), 4895–4907.

Hacker, B. R. (1991), The role of deformation in the formation of metamorphic gradients: Ridge subduction beneath the Oman Ophiolite, *Tectonics*, *10*(2), 455–473.

Hacker, B. R. (1994), Rapid emplacement of young oceanic lithosphere: Argon geochronology of the Oman Ophiolite, *Science*, *265*(5178), 1563–1565.

Hacker, B. R., J. L. Mosenfelder, and E. Gnos (1996), Rapid emplacement of the Oman ophiolite: Thermal and geochronologic constraints, *Tectonics*, *15*(6), 1230–1247.

Hall, C. E., M. Gurnis, M. Sdrolias, L. L. Lavier, and R. D. Müller (2003), Catastrophic initiation of subduction following forced convergence across fracture zones, *Earth Planet. Sci. Lett.*, *212*(1–2), 15–30.

Halliday, A. N., J. P. Davidson, P. Holden, R. M. Owen, and A. M. Olivarez (1992), Metalliferous sediments and the scavenging residence time of Nd near hydrothermal vents, *Geophys. Res. Lett.*, *19*(8), 761–764.

Hanghøj, K., P. B. Kelemen, D. Hassler, and M. Godard (2010), Composition and genesis of depleted mantle peridotites from the Wadi Tayin massif, Oman ophiolite; Major and trace element geochemistry, and Os isotope and PGE systematics, *J. Petrol.*, *51*(1–2), 201–227.

Hart, S. R., J. Blusztajn, H. J. B. Dick, P. S. Meyer, and K. Muehlenbachs (1999), The fingerprint of seawater circulation in a 500-meter section of oceanic crust gabbros, *Geochimica et Cosmochimica Acta*, *33*(23/24), 4059–4080.

Hey, R. (1977), A new class of "pseudofaults" and their bearing on plate tectonics: A propagating rift model, *Earth Planet. Sci. Lett.*, *37*(2), 321–325.

Hofmann, A. W. (2003), Sampling mantle heterogeneity through oceanic basalts: Isotopes and trace elements, in *Treatise on Geochemistry*, edited by D. H. Heinrich, and K. T. Karl, pp. 1–44, Pergamon, Oxford.

Hole, M. J., A. D. Saunders, G. F. Marriner, and J. Tarney (1984), Subduction of pelagic sediments: Implications for the origin of Ce-anomalous basalts from the Mariana Islands, *J. Geol. Soc.*, *141*(3), 453–472.

Ishikawa, T., K. Nagaishi, and S. Umino (2002), Boninitic volcanism in the Oman ophiolite: Implications for thermal condition during transition from spreading ridge to arc, *Geology*, *30*(10), 899–902.

Jaffey, A. H., K. F. Flynn, L. E. Glendenin, W. C. Bentley, and A. M. Essling (1971), Precision measurement of half-lives and specific activities of ^{235}U and ^{238}U, *Phys. Rev. C*, *4*(5), 1889–1906.

Jousselin, D., and A. Nicolas (2000), Oceanic ridge off-axis deep structure in the Mansah region (Sumail massif, Oman ophiolite), *Mar. Geophys. Res.*, *21*(3), 243–257.

Juteau, T., M. Beurrier, R. Dahl, and P. Nehlig (1988a), Segmentation at a fossil spreading axis: The plutonic sequence of the Wadi Haymiliyah area (Haylayn Block, Sumail Nappe, Oman), *Tectonophysics*, *151*(1–4), 167–197.

Juteau, T., M. Ernewein, I. Reuber, H. Whitechurch, and R. Dahl (1988b), Duality of magmatism in the plutonic sequence of the Sumail Nappe, Oman, *Tectonophysics*, *151*(1–4), 107–135.

Karpoff, A. M., A. V. Walter, and C. Pflumio (1988), Metalliferous sediments within lava sequences of the Sumail ophiolite (Oman): Mineralogical and geochemical characterization, origin and evolution, *Tectonophysics*, *151*(1–4), 223–245.

Kelemen, P. B., K. Koga, and N. Shimizu (1997a), Geochemistry of gabbro sills in the crust-mantle transition zone of the Oman ophiolite: Implications for the origin of the oceanic lower crust, *Earth Planet. Sci. Lett.*, *146*(3–4), 475–488.

Kelemen, P. B., G. Hirth, N. Shimizu, M. Spiegelman, and H. J. B. Dick (1997b), A review of melt migration processes in the adiabatically upwelling mantle beneath oceanic spreading ridges, *Philos. Trans. Math. Phys. Eng. Sci.*, *355*(1723), 283–318.

Koepke, J., S. T. Feig, J. Snow, and M. Freise (2004), Petrogenesis of oceanic plagiogranites by partial melting of gabbros: An experimental study, *Contrib. Mineral. Petrol.*, *146*(4), 414–432.

Korenaga, J., and P. B. Kelemen (1997), Origin of gabbro sills in the Moho transition zone of the Oman ophiolite: Implications for magma transport in the oceanic lower crust, *J. Geophys. Res.*, *102*(B12), 27,729–27,749.

Korenaga, J., and P. B. Kelemen (1998), Melt migration through the oceanic lower crust: a constraint from melt percolation modeling with finite solid diffusion, *Earth Planet. Sci. Lett.*, *156*(1–2), 1–11.

Kusano, Y., Y. Adachi, S. Miyashita, and S. Umino (2012), Lava accretion system around mid-ocean ridges: Volcanic stratigraphy in the Wadi Fizh area, northern Oman ophiolite, *Geochem. Geophys. Geosyst.*, *13*, Q05012.

Lanphere, M. A. (1981), K-Ar ages of metamorphic rocks at the base of the Samail ophiolite, Oman, *J. Geophys. Res.*, *86*(B4), 2777–2782.

Lippard, S. J., A. W. Shelton, and I. G. Gass (1986), *The Ophiolite of Northern Oman*, 178 pp., Geological Society, London, London.

MacLeod, C. J., and D. A. Rothery (1992), Ridge axial segmentation in the Oman ophiolite: Evidence from along-strike variations in the sheeted dyke complex, *Geol. Soc. London, Spec. Publ.*, *60*(1), 39–63.

MacLeod, C. J., and G. Yaouancq (2000), A fossil melt lens in the Oman ophiolite: Implications for magma chamber processes at fast spreading ridges, *Earth Planet. Sci. Lett.*, *176*(3–4), 357–373.

MacLeod, C. J., C. J. Lissenberg, L. E. Bibby, J. A. Pearce, K. M. Goodenough, M. T. Styles, and D. J. Condon (2013), Geodynamic setting and origin of the Oman/UAE ophiolite, paper presented at Abstracts of the International Conference on the Geology of the Arabian Plate and the Oman Mountains, Sultan Qaboos University, Muscat, Sultanate of Oman, January 7–9.

Mattinson, J. M. (2005), Zircon U/Pb chemical abrasion (CA-TIMS) method: Combined annealing and multi-step partial dissolution analysis for improved precision and accuracy of zircon ages, *Chem. Geol.*, *220*(1–2), 47–66.

McCulloch, M. T., R. T. Gregory, G. J. Wasserburg, and H. P. Taylor (1981), Sm–Nd, Rb–Sr, and 18O/16O isotopic systematics in an oceanic crustal section: Evidence from the Samail Ophiolite, *J. Geophys. Res.*, *86*(B4), 2721–2735.

McLean, N. M., J. F. Bowring, and S. A. Bowring (2011), An algorithm for U-Pb isotope dilution data reduction and uncertainty propagation, *Geochem. Geophys. Geosyst.*, doi:10.1029/2010GC003478.

Montigny, R., O. Le Mer, R. Thuizat, and H. Whitechurch (1988), K-Ar and Ar study of metamorphic rocks associated with the Oman ophiolite: Tectonic implications, *Tectonophysics*, *151*(1–4), 345–362.

Nicolas, A. (1989), *Structures of Ophiolites and Dynamics of Oceanic Lithosphere*, 367 pp., Kluwer Academic Publishers, London.

Nicolas, A., and F. Boudier (1995), Mapping oceanic ridge segments in Oman ophiolite, *J. Geophys. Res.*, *100*(B4), 6179–6197.

Nicolas, A., and F. Boudier (2003), Where ophiolites come from and what they tell us, *Geol. Soc. Am. Spec. Pap.*, *373*, 137–152.

Nicolas, A., and F. Boudier (2011), Structure and dynamics of ridge axial melt lenses in the Oman ophiolite, *J. Geophys. Res.*, *116*(B3), B03103.

Nicolas, A., F. Boudier, and B. Ildefonse (1996), Variable crustal thickness in the Oman ophiolite: Implication for oceanic crust, *J. Geophys. Res.*, *101*(B8), 17,941–17,950.

Nicolas, A., F. Boudier, B. Ildefonse, and E. Ball (2000), Accretion of Oman and United Arab Emirates ophiolite—Discussion of a new structural map, *Mar. Geophys. Res.*, *21*(3), 147–180.

Nicolas, A., F. Boudier, J. Koepke, L. France, B. Ildefonse, and C. Mevel (2008), Root zone of the sheeted dike complex in the Oman ophiolite, *Geochem. Geophys. Geosyst.*, *9*(5), Q05001.

Olivarez, A. M., and R. M. Owen (1989), REE/Fe variations in hydrothermal sediments: Implications for the REE content of seawater, *Geochim. Cosmochim. Acta*, *53*(3), 757–762.

Pallister, J. S., and C. A. Hopson (1981), Samail ophiolite plutonic suite: Field relations, phase variation, cryptic variation and layering, and a model of a spreading ridge magma chamber, *J. Geophys. Res.*, *86*(B4), 2593–2644.

Pallister, J. S., and R. J. Knight (1981), Rare-earth element geochemistry of the Samail ophiolite near Ibra, Oman, *J. Geophys. Res.*, *86*(B4), 2673–2697.

Pearce, J. A., T. Alabaster, A. W. Shelton, and M. P. Searle (1981), The Oman ophiolite as a Cretaceous arc-basin complex: Evidence and implications, *Philos. Trans. R. Soc. London. Series A, Math. and Phys. Sci.*, *300*(1454), 299–317.

Python, M., and G. Ceuleneer (2003), Nature and distribution of dykes and related melt migration structures in the mantle section of the Oman ophiolite, *Geochem. Geophys. Geosyst.*, *4*(7), 8612.

Python, M., G. Ceuleneer, and S. Arai (2008), Chromian spinels in mafic–ultramafic mantle dykes: Evidence for a two-stage melt production during the evolution of the Oman ophiolite, *Lithos*, *106*(1–2), 137–154.

Rabu, D., F. Béchennec, M. Beurrier, and G. Hutin (1986), Nakhl-Sheet NF40-3E Geologic Map, Ministry of Petroleum and Minerals, Directorate General of Minerals, Sultanate of Oman.

Reagan, M. K., et al. (2010), Fore-arc basalts and subduction initiation in the Izu-Bonin-Mariana system, *Geochem. Geophys. Geosyst.*, *11*(3), Q03X12.

Reuber, I. (1988), Complexity of the crustal sequence in the northern Oman ophiolite (Fizh and southern Aswad blocks): The effect of early slicing?, *Tectonophysics*, *151*(1–4), 137–165.

Reuber, I., P. Nehlig, and T. Juteau (1991), Axial segmentation at a fossil oceanic spreading centre in the Haylayn block (Semail nappe, Oman): Off-axis mantle diapir and advancing ridge tip, *J. Geodyn.*, *13*(2–4), 253–278.

Rioux, M., S. A. Bowring, P. B. Kelemen, S. Gordon, F. Dudás, and R. Miller (2012a), Rapid crustal accretion and magma assimilation in the Oman-U.A.E. ophiolite: High precision U-Pb zircon geochronology of the gabbroic crust, *J. Geophys. Res.*, *117*, B07201, doi:10.1029/2012JB009273.

Rioux, M., C. J. Lissenberg, N. M. McLean, S. A. Bowring, C. J. MacLeod, E. Hellebrand, and N. Shimizu (2012b), Protracted timescales of lower crustal growth at the fast-spreading East Pacific Rise, *Nat. Geosci.*, doi:10.1038/NGEO1378.

Robertson, A. H. F., and A. J. Fleet (1986), Geochemistry and palaeooceanography of metalliferous and pelagic sediments from the Late Cretaceous Oman ophiolite, *Mar. Pet. Geol.*, *3*(4), 315–337.

Rollinson, H. (2009), New models for the genesis of plagiogranites in the Oman ophiolite, *Lithos*, *112*(3–4), 603–614.

Searle, M., and J. Cox (1999), Tectonic setting, origin, and obduction of the Oman ophiolite, *Geol. Soc. Am. Bull.*, *111*(1), 104–122.

Searle, M., and J. Cox (2002), Subduction zone metamorphism during formation and emplacement of the Semail ophiolite in the Oman Mountains, *Geol. Mag.*, *139*(3), 241–255.

Searle, M. P., and J. Malpas (1980), The structure and metamorphism of rocks beneath the Semail Ophiolite of Oman and their significance in ophiolite obduction, *Trans. R. Soc. Edinburgh: Earth Sci.*, *71*, 247–262.

Searle, M. P., and J. Malpas (1982), Petrochemistry and origin of sub-ophiolitic metamorphic and related rocks in the Oman Mountains, *J. Geol. Soc. (London)*, *139*(3), 235–248.

Searle, M. P., S. J. Lippard, J. D. Smewing, and D. C. Rex (1980), Volcanic rocks beneath the Semail Ophiolite nappe in the northern Oman mountains and their significance in the Mesozoic evolution of Tethys, *J. Geol. Soc. (London)*, *137*(5), 589–604.

Smewing, J. D. (1981), Mixing characteristics and compositional differences in mantle-derived melts beneath spreading axes: Evidence from cyclically layered rocks in the ophiolite of North Oman, *J. Geophys. Res.*, *86*(B4), 2645–2659.

Stakes, D. S., and H. P. Taylor (2003), Oxygen isotope and chemical studies on the origin of large plagiogranite bodies in northern Oman, and their relationship to the overlying massive sulphide deposits, *Geol. Soc. London, Spec. Publ.*, *218*(1), 315–351.

Stern, R. J. (2004), Subduction initiation: Spontaneous and induced, *Earth Planet. Sci. Lett.*, *226*(3–4), 275–292.

Stern, R. J., and S. H. Bloomer (1992), Subduction zone infancy: Examples from the Eocene Izu-Bonin-Mariana and Jurassic California arcs, *Geol. Soc. Am. Bull.*, *104*(12), 1621–1636.

Tamura, A., and S. Arai (2006), Harzburgite-dunite-orthopyroxenite suite as a record of supra-subduction zone setting for the Oman ophiolite mantle, *Lithos*, *90*(1–2), 43–56.

Tilton, G. R., C. A. Hopson, and J. E. Wright (1981), Uranium-lead isotopic ages of the Samail ophiolite, Oman, with applications to Tethyan ocean ridge tectonics, *J. Geophys. Res.*, *86*(B4), 2763–2775.

Valsami-Jones, E., and J. R. Cann (1994), Controls on the Sr and Nd isotopic compositions of hydrothermally altered rocks from the Pindos Ophiolite, Greece, *Earth. Planet. Sci. Lett.*, *125*(1–4), 39–54.

Villey, M., X. de Gramont, and J. Le Métour (1986), Fanjah-Sheet NF40-3F Geologic Map, Ministry of Petroleum and Minerals, Directorate General of Minerals, Sultanate of Oman.

Warren, C., R. Parrish, D. Waters, and M. Searle (2005), Dating the geologic history of Oman's Semail ophiolite: Insights from U-Pb geochronology, *Contrib. Mineral. Petrol.*, *150*(4), 403–422.

Warren, C., M. Searle, R. Parrish, and D. Waters (2007), Reply to Comment by F. Boudier and A. Nicolas on "Dating the geologic history of Oman's Semail Ophiolite: Insights from U–Pb geochronology" by C.J. Warren, R. R. Parrish, M.P. Searle and D.J. Waters, *Contrib. Mineral. Petrol.*, *154*(1), 115–118.